August 2015

Predictability of Sea Ice Near Bifurcations

Dawn Marie Kopacz
University of Wisconsin-Milwaukee

PREDICTABILITY OF SEA ICE NEAR BIFURCATIONS

by

Dawn Kopacz

A Dissertation Submitted in

Partial Fulfillment of the

Requirements for the Degree of

Doctor of Philosophy

in Mathematics

at

The University of Wisconsin – Milwaukee

August 2015

ABSTRACT
PREDICTABILITY OF SEA ICE NEAR BIFURCATIONS

by

Dawn Kopacz

The University of Wisconsin – Milwaukee, 2015
Under the Supervision of Professor Kyle Swanson

There is evidence in Earth's history of relatively stable climate regimes abruptly transitioning to alternative states. It has been argued that the greatest potential for such abrupt transitions in Earth's system in the near future is located in the Arctic. Here we analyze the Arctic sea ice evolution of two current generation climate models that exhibit critical transitions. We demonstrate the detectability of two early warning signals: increased variance and increased autocorrelation. We introduce another metric that forewarns of abrupt changes in sea ice; a decrease in predictability before the threshold points. Observations of Arctic sea ice extent are searched for early warning signals using methods identical to the model analysis. A regional analysis is also performed for both models and observations and demonstrates that these metrics are detectable at the regional level. We show that the complexities of the Arctic sea ice system can be reduced to a simple stochastic sea ice model and determine that our warning metrics are applicable in that setting as well.

Because there is often little to no change to the state of the system before an abrupt change, the robustness of these metrics make them promising indicators of the risk of upcoming regime shifts in the Arctic sea ice system. But given the decrease in predictability of sea ice near a bifurcation, an improved understanding of the physical mechanisms forcing abrupt climate change is needed if we are to improve sea ice forecasts moving forward. Understanding the reason behind the vastly different outcomes produced by the climate models may help us with this task.

TABLE OF CONTENTS

		Page
Title page		i
Abstract		ii
List of Figures		vii
List of Tables		xii
CHAPTER		
1	Introduction	1
2	Data and methods	8
	2.1 Models	8
	2.2 Observations	10
	2.3 Autocorrelation at lag-1 and variance	11
	2.3.1 Models	11
	2.3.2 Observations	15
	2.4 Surrogate data	15
	2.4.1 Models	15
	2.4.2 Observations	17
	2.5 Forecast skill metric	17
	2.5.1 Models	17
	2.5.2 Observations	19
3	Early warning signals	19

Page

3.1 Lag-1 autocorrelation method 19

3.1.1 Models 19

3.1.2 Observations 21

3.2 Forecast skill metric 21

3.2.1 Models 21

3.2.2 Observations 23

4 Regional early warning signals 24

4.1 Identification of distinct regions of abrupt change 24

4.2 Lag-1 autocorrelation method: Regional analysis 26

4.2.1 Models 26

4.2.2 Observations 27

4.3 Forecast skill metric: Regional analysis 28

4.3.1 Models 28

4.3.2 Observations 30

5 Stochastic sea ice model 31

5.1 Model results 35

5.2 Lag-1 autocorrelation method 37

5.3 Forecast skill metric 39

6 Sea ice albedo feedback as a driver of abrupt change 40

7 Discussion and Conclusions 42

Page

8 Future work 45

Figures 47

Table 1 84

References 85

Appendix – MATLAB code for stochastic sea ice model 88

Curriculum Vitae 93

LIST OF FIGURES

FIGURE Page

1. Schematic of the thermodynamic and dynamic (v_{ice}) components of the sea ice ocean atmosphere system. 47

2. Schematic of system response to small perturbations. A small change in forcing usually results a smooth, gradual and reversible response to the system. In case (b), small changes in forcing result in disproportionately large changes to the system, but remain reversible. In panel (c), small changes have resulted in an abrupt shift in the state of the system (critical transition). The right panel shows how small perturbations to the system can appear to have no effect, until the system nears the tipping point. The resilience of the system decreases (basin of attraction shrinks) until the point where even a tiny perturbation causes a critical transition. Figure is borrowed from the following website: http://www.early-warning-signals.org/theory/what-is-a-critical-transition/ and was developed by SparcS Center (Scheffer et al. 2015). 48

3. September sea ice extent ($mil.km^2$) averaged over 40°N to 90°N for the MIROC-ESM-CHEM (red) and FIO-ESM (blue) models for the period 1861-2100. 49

4. Sea ice extent ($mil.km^2$) and surface temperature (°C) averaged over 40°N to 90°N for the MIROC-ESM-CHEM model for September from 1861-2100 and 1850-2100 respectively. 50

5. Sea ice extent ($mil.km^2$) and surface temperature (°C) averaged over 40°N to 90°N for the FIO-ESM model for March from 1861-2100 and 1850-2100 respectively. 51

6. Observed sea ice extent anomaly and surface temperature anomaly (°C) averaged over 40°N to 90°N for September from 1979-2013 and 1880-2014 respectively. 52

FIGURE Page

7. Sea ice extent anomalies (relative to 1901-1950 mean; $mil.km^2$) averaged over 40°N to 90°N for the MIROC-ESM-CHEM model from 1861 to 2100 (grey line). Autocorrelation coefficients (AR; blue line) and variance (VAR; red line), measured as the standard deviation, for a window size of 35 years. Thick, black vertical line denotes the transition year (2016). 53

8. Sea ice extent anomalies (relative to 1901-1950 mean; $mil.km^2$) averaged over 40°N to 90°N for the FIO-ESM model from 1861 to 2100 (grey line). Autocorrelation coefficients (AR; blue line) and variance (VAR; red line), measured as the standard deviation, for a window size of 35 years. Thick, black vertical line denotes the transition year (2064). 54

9. Observed sea ice extent anomalies (relative to 1951-1980 mean; $mil.km^2$) averaged over 40°N to 90°N for the period 1979-2013 (grey line). Autocorrelation coefficients (AR; blue line) and variance (VAR; red line), measured as the standard deviation, for a window size of 16 years. 55

10a. MIROC-ESM-CHEM September sea ice extent ($mil.km^2$) averaged over 40°N to 90°N (grey line). Blue line is the forecast skill (relative to a CLIPER forecast) for the month of September, averaged over all analog forecast periods. 56

10b. Mean skill relative to climatology for an analog forecast (red) and CLIPER forecast (blue) for MIROC-ESM-CHEM September sea ice extent. 57

11a. FIO-ESM March sea ice extent ($mil.km^2$) averaged over 40°N to 90°N (grey line). Blue line is the forecast skill (relative to a CLIPER forecast) for the month of March, averaged over all analog forecast periods. 58

11b. Mean skill relative to climatology for an analog forecast (red) and CLIPER forecast (blue) for FIO-ESM March sea ice extent. 59

FIGURE Page

12. Observed September sea ice extent anomaly ($mil.km^2$) averaged over 40°N to 90°N (black line). Blue line is the mean skill (relative to a CLIPER forecast) for all analog forecast periods. 60

13a. Arctic Ocean sub-region used for the regional analysis of the MIROC-ESM-CHEM model. 61

13b. Greenland Sea sub-region used for the regional analysis of the FIO-ESM model. 62

14. Sea ice extent ($mil.km^2$) and surface temperature (°C) averaged over the Arctic Ocean for the MIROC-ESM-CHEM model for September from 1861-2100 and 1850-2100 respectively. 63

15. Sea ice extent ($mil.km^2$) and surface temperature (°C) averaged over the Greenland Sea for the FIO-ESM model for March from 1861-2100 and 1850-2100 respectively. 64

16. Observed sea ice extent anomaly and surface temperature anomaly (°C) averaged over the Arctic Ocean for September from 1979-2013 and 1880-2014 respectively. 65

17. Sea ice extent anomalies (relative to the 1901-1950 mean; $mil.km^2$) averaged over the Arctic Ocean for the MIROC-ESM-CHEM model from 1861 to 2100 (grey line). Autocorrelation coefficients (AR; blue line) and variance (VAR; red line), measured as the standard deviation, for a window size of 35 years. Thick, black vertical line denotes the transition year (2016). 66

18. Sea ice extent anomalies (relative to the 1901-1950 mean; $mil.km^2$) averaged over the Greenland Sea for the FIO-ESM model from 1861 to 2100 (grey line). Autocorrelation coefficients (AR; blue line) and variance (VAR; red line), measured as the standard deviation, for a window size of 35 years. Thick, black vertical line denotes the transition year (2064). 67

FIGURE Page

19. Observed sea ice extent anomalies (relative to the 1950-1981 mean; $mil.km^2$) averaged over the Arctic Ocean for the period 1979-2013 (grey line). Autocorrelation coefficients (AR; blue line) and variance (VAR; red line), measured as the standard deviation, for a window size of 16 years. 68

20a. MIROC-ESM-CHEM September sea ice extent ($mil.km^2$) averaged over the Arctic Ocean (grey line). Blue line is the forecast skill (relative to climatology) for the month of September, averaged over all analog forecast periods. 69

20b. MIROC-ESM-CHEM February sea ice extent ($mil.km^2$) averaged over the Arctic Ocean (grey line). Blue line is the forecast skill (relative to climatology) for the month of February, averaged over all analog forecast periods. 70

21. FIO-ESM March sea ice extent ($mil.km^2$) averaged over Greenland (grey line). Blue line is the forecast skill (relative to climatology) for the month of March, averaged over all analog forecast periods. 71

22. Observed September sea ice extent anomaly ($mil.km^2$) averaged over the Arctic Ocean (grey line). Blue line is the mean skill (relative to a CLIPER forecast) for all analog forecast periods. 72

23. Schematic of the thermodynamic and dynamic [$v_0\ R(-E)$] components of the stochastic sea ice model used in this study, which is a single column representation of the atmosphere, sea ice and ocean mixed layer. 73

24. Diagram showing the bifurcation behavior within the stochastic sea ice model (Figure 3 from EW09). For each value of the imposed surface flux ΔF_o, the model is run until is converges on a steady-state seasonal cycle. The annual maximum and minimum values of E ($W\ m^{-2}\ yr$) are plotted (right axis). The corresponding sea ice thickness in meters (h_i) or ocean mixed layer temperature in ℃ (T_{ml}) are plotted on the left axis.
The blue lines indicate perennial sea-ice conditions, the solid red lines indicate seasonally ice-free solutions, dashed red lines indicate unstable solutions and perennially ice-free conditions are marked by the grey lines. 74

FIGURE Page

25a. Sample solution produced by the stochastic sea ice model with the following parameters: $\Delta F_o = 22.25\ Wm^{-2}, E(1,1) = 0\ Wm^{-2}\ yr$ and $S = 0\ Wm^{-2}$. 75

25b. Sample solution produced by the stochastic sea ice model with the following parameters: $\Delta F_o = 22.25\ Wm^{-2}, E(1,1) = 30\ Wm^{-2}\ yr$ and $S = 0\ Wm^{-2}$. 76

25c. Sample solution produced by the stochastic sea ice model with the following parameters: $\Delta F_o = 22.25\ Wm^{-2}, E(1,1) = 13\ Wm^{-2}\ yr$ and $S = 1\ Wm^{-2}$. 77

25d. Sample solution produced by the stochastic sea ice model with the following parameters: $\Delta F_o = 22.25\ Wm^{-2}, E(1,1) = 13\ Wm^{-2}\ yr$ and $S = 1\ Wm^{-2}$. 78

26a. Average of the ten time series from the stochastic sea ice model, which exhibit a rapid transition to an ice-free state (centered on the transition point; grey line). Blue line is the lag-1 autocorrelation for a window size of 7 years. 79

26b. Average of the ten time series from the stochastic sea ice model which exhibit a rapid transition to an ice-free state (centered on the transition point; grey line). Red line is the standard deviation for a window size of 7 years. 80

27. Average of the ten time series from the stochastic sea ice model which exhibit a rapid transition to an ice-free state (grey line). Red line is the mean skill (relative to climatology) for all analog forecast periods. 81

28a. Arctic surface albedo, estimated using the ratio of reflected shortwave radiation in the upward (rsus) and downward (rsds) directions, respectively. Thick, black vertical lines denote the year of sea ice transition in the MIROC-ESM-CHEM and FIO-ESM models respectively. 82

28b. As in Figure 28a; modeled Arctic albedo (top of atmosphere). 83

LIST OF TABLES

TABLE Page

1. Definitions and magnitudes of stochastic sea ice model parameters. For the three seasonally varying parameters $F_0(t)$, $F_T(t)$ and $F_s(t)$, the table value is the annual average; the monthly means for January through December are:
$F_0(t) = [120\ 120\ 130\ 94\ 64\ 61\ 57\ 54\ 56\ 64\ 82\ 110]\ \mathrm{W\,m^{-2}}$,
$F_T(t) = [3.1\ 3.2\ 3.3\ 2.9\ 2.6\ 2.6\ 2.5\ 2.5\ 2.6\ 2.7\ 3.1]\ \mathrm{W\,m^{-2}\,K^{-1}}$ and
$F_s(t) = [0\ 0\ 30\ 160\ 280\ 310\ 220\ 140\ 59\ 6.4\ 0\ 0]\ \mathrm{W\,m^{-2}}$. 84

1 Introduction

There is a decreasing trend in observed Arctic sea ice extent for all months since the start of the satellite record. Over much of the last decade, the reduction in Arctic sea ice has accelerated, with September sea ice extent reaching several extreme minima since 2002 (Boe et al. 2009; Bekryaev et al. 2010; Stroeve et al. 2011). This raises the question of whether a collapse in sea ice looms in the near future. However, there are significant challenges to forecasting such an abrupt change. This is because small changes in external conditions may result in disproportionally large changes to the state of the system (Scheffer et. al 2009). This is complicated by a broad range of model projections of the Arctic climate that leave us with a lack of guidance as to the future of Arctic sea ice.

Sea ice is a complex climate sub-system to model, but it is necessary to our understanding of future climate change. Sea ice significantly alters the albedo of the ocean surface, causes salinity changes during the freezing and melting process and the presence of sea ice inhibits the exchange of heat, moisture and momentum between the atmosphere and the ocean. In addition to thermodynamic processes that affect the growth and melt of sea ice, there are dynamic processes such as wind and ocean currents that cause deformation of the ice and transport of sea ice out of the Arctic. Furthermore, because the heat and moisture fluxes that influence the atmospheric circulation and precipitation patterns of the Arctic are strongly linked to sea ice, accurate models of Arctic sea ice are also necessary for successful forecasts of the global climate (Trenberth 1992).

To accurately model sea ice, we must understand the how sea ice forms and the processes that cause it to grow and decay. Sheets of sea ice form when small ice crystals form and bond together. Under calm conditions, these ice crystals form into a thin, continuous sheet of ice that thickens when one or more of these ice sheets collide and slide over each other (rafting). In rough ocean waters, the ice crystals collect into mushy circular disks called pancake ice and are characterized by ridges around their edges as the disks bump into one another. Eventually the collisions are strong enough to combine several disks into a single ice sheet with rough surfaces.

Figure 1 outlines the basics of a single column representation of the atmosphere, sea ice and ocean mixed layer. Ice growth begins during autumn when the incoming solar radiation, F_{solar}, decreases and the cold air causes the upper layer of the ocean surface to cool to the freezing point of seawater ($\sim -2℃$). As the density of the water increases, the cold water sinks and is replaced by warmer water. Surface energy fluxes ($F_{surface}$) continue to remove heat from the ocean to the atmosphere and the process of ice formation begins. The presence of sea ice alters the surface albedo (α) and amplifies the surface cooling when ice is present. Additional thermodynamic variables that affect the surface temperature and therefore the growth or decay of sea ice are atmospheric energy transport into the Arctic (F_{south}) and heat fluxes into the bottom of the sea ice which cause melting from below (F_{bottom}). Outgoing longwave radiation is typically specified as a linear function of surface temperature ($A + BT$), where the coefficients A and B are obtained from theoretical or observationally based estimates.

The insulating properties of sea ice inhibit heat transfer as it grows thicker. Therefore, thin ice grows rapidly, with the ice growth rate slowing as the thickness

increases. If the ice grows thick enough that essentially no heat is conducted from the ocean to the atmosphere, then the ice growth ceases. This is known as thermodynamic equilibrium and the equilibrium thickness in the Arctic is roughly three meters, though deformation can produce sea ice thicker than ten meters (Hartmann 1994; Trenberth 1992).

As solar energy increases in the spring and summer, surface temperatures rise and the ice begins to melt from above and below. Thin ice will melt completely during the spring and summer, but thick ice may persist from year to year, thinning during the summer and thickening again through autumn and winter. In addition to the thermodynamic processes that cause ice to melt, dynamic processes such as wind and ocean currents remove ice from the system (v_{ice}). Ice flows southward through the Fram Strait, melting when it reaches the Greenland and Norwegian Seas and acting to cool the ocean in these source regions of deep water for the world's oceans.

Complex dynamical systems like Arctic sea ice often have critical thresholds at which the system abruptly transitions to an alternative stable state, called a "tipping point" (Scheffer et. al 2009). The non-linearity of Earth's climate system suggests that abrupt changes are possible, and in fact, past climate records provide examples of regime shifts such as the greenhouse-icehouse transition and the end of the Younger Dryas period (Cuffy et. al 1997; Dakos et. al 2008; Scheffer et. al 2009). It has been argued that the greatest potential for abrupt transitions in Earth's system today is located in the Arctic, most pressingly a collapse in Arctic sea ice (Duarte et. al 2012).

Given the non-linear dynamics of the Arctic sea ice system and the current rapid rate of sea ice loss, the potential for a tipping point within the Arctic sea ice system is a topic of significant interest in the scientific community (Abbot et al. 2011; Thompson & Sieber 2011). Mathematical theory defines tipping points as catastrophic bifurcations, of which there are several different types. One of the most recognized cases is a fold catastrophe, which can be described by the change in the equilibrium state of the system in response to a change in conditions (left panel of Figure 2). Usually, a small perturbation to the system results in a smooth, gradual and reversible response within the system (Box a), but it can also cause a disproportionately large change to the system that remains reversible (Box b). Critical transitions arise when the equilibrium curve becomes "folded" (Box c). At this point, small changes can result in an abrupt shift in the state of the system (critical transition). The right panel of Figure 2 shows how small perturbations to the system can appear to have no effect, until the system nears the tipping point. The resilience of the system, or its ability to absorb a perturbation without abruptly transitioning is illustrated by the width and gradient of the wells in the right panel of Figure 2. Conditions continue to bring the system closer to the transition point and as this happens, the system becomes less resilient, eventually decreasing to the point where even a tiny perturbation causes a critical transition (Scheffer et al. 2015).

In applied mathematics involving differential equations, such as the modeling of Arctic sea ice, the ordinary differential equations (ODEs) have parameters that are often approximated, making it important to study the changes in the qualitative behavior of the system as one or more of these parameters vary (van Voorn 2006). Bifurcation theory becomes relevant because a slight variation in a parameter can have a significant impact

on the solution of the ODE, for example, the evolution of sea ice within a model. Prior to a critical transition, a system may undergo stochastic fluctuations around a stable, fixed point and appear be at equilibrium, but a slowly changing external parameter can put the system at risk of undergoing a critical transition.

Previous studies have shown that there are generic properties that describe the dynamics of a dynamical system as it nears a bifurcation point (Dakos et. al. 2008; Scheffer et. al. 2009; van Nes and Scheffer 2007; Lenton 2012). These properties have been appropriately termed "early warning signals". Perhaps the most recognizable indicator of an impending transition is a phenomenon known as "critical slowing down," where once disturbed the system becomes slow to return to equilibrium. An increase in short-time period (or lag-1) autocorrelation prior to the transition point is an indicator of the system's increased memory (Scheffer et. al. 2009). An increase in variance is another early warning indicator, and it has been suggested that this metric is equally important in diagnosing the threat of an impending bifurcation (Ditlevsen and Johnsen 2010).

Here, the potential for early warning signals in Arctic sea ice is studied using observations and models. The time series of two global climate models found at opposite ends of the model spectrum in terms of sea ice behavior are examined at length, and an observational sea ice extent time series are searched for an increase in autocorrelation as well as an increase in variance (measured as the standard deviation), to determine if the metrics can be used as early warning signals of a transition in Arctic sea ice behavior. A short-term analog sea ice forecast is developed for both the models and observations and demonstrates skill over climatology and a CLIPER (climatology + persistence) forecast. These various measures of forecast skill provide additional early warning indicators for

abrupt sea ice transitions. These techniques are then applied to an observed sea ice time series. Similar analyses are performed at the regional scale to determine whether early warning indicators are detectable at the regional level.

These empirical studies are augmented by the study of an idealized model of sea ice following Eisenman and Wettlaufer (hereafter EW09). They introduced a sea ice ocean atmosphere model that produces a simulation of the Arctic sea ice seasonal cycle that is consistent with observations to investigate the physical mechanisms behind potential bifurcation behavior in the Arctic sea ice system. Here we recreate the idealized Arctic sea ice ocean atmosphere model and investigate its bifurcation behaviors and the predictability of sea ice within the model. An early warning signal analysis is performed to determine whether our warning metrics are detectable in this simplified model. A novel aspect of this analysis is the study of spontaneous transitions in the absence of formal parameter variations for this idealized system.

Truly meaningful predictions of Arctic sea ice continue to be limited by our lack of understanding of the physical mechanisms forcing abrupt changes within the Arctic system (Bekryaev et al., 2010). Given the substantial range in model projections of the future Arctic climate and the role of the Arctic in global climate change, determining what is causing these differences in simulated Arctic climate is crucial (Boe et al., 2009). The sea ice albedo feedback (SIAF) is often cited as the strongest contributor to high latitude climate change, and more importantly accelerated changes. The reduction of snow and ice due to anthropogenic induced warming leads to more open land and water, which decreases the albedo and increases solar absorption, inducing a further increase in temperature, eventually propelling the system into a stable, ice-free state (Holland and

Bitz 2003; Hall 2003; Curry and Schramm 1994; Manabe and Stouffer 1980). Alternatively, with a decrease in temperature, the SIAF would lead to more ice and snow, an increased surface albedo and further cooling. Budyko and Sellers separately incorporated the ice albedo feedback effect into simple energy balance models. Both of their models assumed that the surface temperature could characterize everything about the climate and the resultant model climates were very sensitive, with the SIAF giving rise to nonlinear climate changes within their models (Hartmann 1994).

Given that a critical threshold for summer Arctic sea ice loss may occur in the near future and changes to the Arctic sea ice system provide economic prospects to some local communities while threatening others, diagnosing the risk of an impending collapse as well as understanding the dynamical causes of such a collapse is necessary. Furthermore, due to the strong feedbacks associated with sea ice, realistic predictions of the global climate also depend on adequate projections of the future of Arctic sea ice (Juricke et al. 2014; Kattsov et al. 2010). The relative importance of the SIAF to the rapid sea ice changes within the global climate models used in our analysis is also investigated. The ratio of upward to downward reflected radiation at the surface and top of the atmosphere is used to estimate the albedo for each model in an effort to understand the differences in model outcomes.

2 Data and Methods

2.1 Models

Model projections are taken from phase five of the Coupled Model Intercomparison Project (CMIP5) multi-model ensemble carried out in support of the Intergovernmental Panel on Climate Change Fifth Assessment Report (IPCC AR5). Unlike IPCC's AR4 Special Report on Emissions Scenarios (SRES), the CMIP5 multi-model ensemble is divided into four scenarios to illustrate a large assortment of potential future climate projections. Called Representative Concentration Pathways (RCPs), the scenarios are numbered according to their radiative forcing level in the year 2100 and include gridded information on land use and short-lived sulfate aerosol emissions, as well as long-lasting greenhouse gas emissions. The RCP 2.6 scenario has a radiative forcing level that peaks around 3.1 W/m^2 mid-century, and returns to 2.6 W/m^2 by 2100. This is consistent with mitigation strategies that have a target limit of a 2˚C increase in global mean temperature (van Vuuren et al. 2007).

The model data record for the simulations examined here begins in 1861 and ends in 2100. When evaluating the model's risk of a rapid shift, anomalies relative to the 1901-1950 mean are used. Raw data is used for the short-term forecast analysis. The model sea ice data is given as a percent concentration, or the fraction of sea ice covering each grid cell. Multiplying the fraction of sea ice in each grid cell (SIC) by the area of the grid cell (A) and weighting by the cosine of the latitude (lat) at each location, converts the quantity to sea ice extent. Only grid cells with greater than 15% sea ice concentration were included.

The sea ice extent times series (extent) is the sum of all of those grid cell extent values from $40°N$ latitude to the North Pole, for each month in the record:

$$extent = \sum_{lat_{min}}^{lat_{max}} SIC(lat) * A * \cos(lat) \qquad (1)$$

There is a broad range of future sea ice scenarios produced by the CMIP5 multi-model ensemble. The MIROC-ESM-CHEM (Japanese) and FIO-ESM (Chinese) models are found at opposite ends of the model spectrum, with other model simulations bounded by these two scenarios. Figure 3 shows the model sea ice extent for both models during the month of September. We can see that the model mean sea ice concentrations are very similar until roughly the year 2000, after which both models exhibit large deviations from their mean in previous years.

The MIROC-ESM-CHEM surface air temperatures (1850-2100) and September sea ice extent (1861-2100) from 40°N to 90°N latitude are displayed in Figure 4. This model exhibits a significant rise in surface temperatures across the Arctic region and a rapid loss of sea ice, with all but a few of the Septembers after 2050 being virtually, if not completely, ice free. A threshold is reached in 2016 that shifts the system to a contrasting state and the sea ice extent sharply declines during the subsequent four years, exhibiting an 88.5% drop in sea ice extent (catastrophic bifurcation; Scheffer et. al 2009).

In contrast, the FIO-ESM model exhibits Arctic cooling in the latter part of the 21st century (Figure 5). Unlike the MIROC-ESM-CHEM model, the FIO-ESM model sea ice values remain relatively stable until approximately 2040, at which point the sea ice extent

begins to increase steadily, with an abrupt jump in the year 2064. This model displays a nearly 14% increase in sea ice in just five years, with the sea ice extent peaking at roughly 38% above the average sea ice extent prior to the year 2040 near the end of the record.

The transition points discussed above were determined through a combination of visual analysis and percent change calculations. Visually, the transition point was identified as the point at which the sea ice extent began its rapid shift away from the prior long-term mean (2016 and 2064 for the MIROC-ESM-CHEM and FIO-ESM, respectively). Based upon this transition time, we then calculated the percent change in sea ice extent in the four (five) years after the proposed transition point in the MIROC-ESM-CHEM (FIO-ESM) sea ice record. Both models experienced a considerable percent change in sea ice concentration in that period, confirming our visual diagnosis of the transition points.

2.2 Observations

Surface air temperature anomalies were obtained from the National Aeronautics and Space Administration (NASA), Goddard Institute for Space Studies (GISS). Surface air temperature anomalies on a $2° \, x \, 2°$ global grid with 250 kilometer smoothing cover the period 1880-2014. We area-averaged the data from 40°N to 90°N latitude and computed anomalies relative to the 1951-1980 mean. Surface air temperatures have risen rapidly in the last few decades (since about 1980), with multiple surface temperature maximums observed since the year 2000 (Figure 6; grey line).

The NASA Goddard Space Flight Center (GSFC) Oceans and Ice Branch provides the sea ice observations to the National Snow and Ice Data Center (NSIDC), where we obtained monthly sea ice extent anomalies spanning the period 1979-2013. Brightness temperature data from the Nimbus-7 Scanning Multichannel Microwave Radiometer (SMMR), Special Sensor Microwave/Imagers (SMM/Is) and Special Sensor Microwave Imager/Sounder (SSMIS) are used to derive the data. A consistent time series of sea ice extent spanning the coverage of several passive microwave instruments is produced using the NASA Team algorithm developed by the Oceans and Ice Branch, Laboratory for Hydrospheric Processes (Cavalieri et. al. 1996).

The data consists of monthly anomalies of total sea ice extent from January 1979 through December 2013 for all longitudes north of approximately 40°N latitude. Data was missing for December 1987, so it was replaced with the average of the sea ice extent in the two months before and two months after the missing data point. Figure 6 shows the sea ice extent anomalies for the month of September from 1979-2013 (black line). We can see from the figure that there is a steady decline in the observed sea ice extent, with two extreme minima observed in September 2007 and 2012.

2.3 Autocorrelation at lag-1 and variance

2.3.1 Models

As a critical transition is approached, the return rate to equilibrium decreases causing the short-term memory of the system to increase ahead of the transition (critical slowing down; Scheffer et. al 2009). Increased short-term memory within the system means that the system becomes less resilient. As the transition point is neared, the system will take

longer to return to equilibrium, even after small perturbations. This slowing down typically starts far from the bifurcation point and can be shown mathematically by considering the following simple dynamical system, with parameters a and b, and γ is a positive scaling factor,

$$\frac{dx}{dt} = f(x) = \gamma(x-a)(x-b), \qquad (2)$$

with equilibrium points at $\bar{x}_1 = a$ (stable) and $\bar{x}_2 = b$ (unstable). Examining the stable equilibrium as it is perturbed slightly ($x = \bar{x}_1 + \varepsilon$), linearizing and simplifying we have the following:

$$\frac{d(\bar{x}_1+\varepsilon)}{dt} = f(\bar{x}_1+\varepsilon) \approx f(\bar{x}_1) + \left.\frac{\partial f}{\partial x}\right|_{\bar{x}_1} \varepsilon = f(\bar{x}_1) + \frac{d\varepsilon}{dt} \qquad (3)$$

where $\frac{d\varepsilon}{dt} = \lambda\varepsilon$ and the eigenvalues λ_1 and λ_2 defined as

$$\lambda_1 = \gamma(a-b) \quad and \quad \lambda_2 = \gamma(b-a), \qquad (4)$$

where λ_1 represents the recovery rate for the stable equilibrium point $\bar{x}_1$ and λ_2 is the recovery rate for $\bar{x}_2$. Equation (4) demonstrates that when $a = b$, the recovery rates are both equal to zero and the system will not recover from perturbations and a bifurcation occurs.

This dynamical slowing down will tend to lead to an increase in lag-1 autocorrelation prior to the transition point and is an indicator of the system's increased memory (Scheffer et. al. 2009). An increase in variance is another early warning indicator, and it has been suggested that this metric is equally important in diagnosing the threat of an impending bifurcation (Ditlevsen and Johnsen 2010). It is suggested that it is possible to reduce the dynamics of a system to a one-dimensional time series modeled by a linear first-order autoregressive (AR-1) process if the time step Δt is fixed (Scheffer et. al 2009; van Nes and Scheffer 2007):

$$y_{n+1} = \alpha y_n + \sigma \varepsilon_n, \tag{5}$$

where ε_n is Gaussian white noise and $\alpha = e^{\lambda \Delta t}$ with λ defined as the recovery rate at which the system returns to equilibrium after recurrent disturbances. This means that when the system moves away from equilibrium and the return rate increases, the autocorrelation will tend to one.

The variance of the AR-1 process described in Equation (5) can be determined as follows:

$$Var(y_{n+1}) = E(y_{n+1}^2) - \mu^2 = \frac{\sigma^2}{(1-\alpha^2)}, \tag{6}$$

which demonstrates that the critical slowing down as the transition point is approached causes the recovery rate to equilibrium (λ) to decrease, the autocorrelation (α) tends to one and the variance will approach infinity.

For the climate models used in this analysis, we estimated the lag-1 autocorrelation and the variance (measured as the standard deviation) within a rolling window. Since the search for these warning signals in observed data would require that the indicators be estimated as the data becomes available, we used an overlapping, moving window. The window size was varied from 20 to 100 years, with the most significant trends observed with the largest window sizes, but we chose to use a sliding window (win) of 35 years as this provided a clear trend while remaining observationally relevant.

The autocorrelation at lag-1 and the variance were calculated up to but not including the bifurcation point for each modeled sea ice extent data set ($extent$). The lag-1 autocorrelation coefficients (AR) at each time step (t) were computed as follows,

$$AR(t) = \frac{cov(x,y)}{\sigma_x * \sigma_y} \qquad (7)$$

$$where \qquad x = extent(t : t + win)\,, \quad y = extent(t-1 : t-1+win),$$

$$cov(x,y) = (\sum_{i=1}^{N} \frac{(x_i - \bar{x})(y_i - \bar{y})}{N} \qquad and \qquad \sigma_x = \left(\frac{1}{N-1}\sum_{i=1}^{N}(x_i - \bar{x})^2\right)^{\frac{1}{2}}$$

To avoid bias in our autocorrelation estimate, we were careful not to include points that were part of the transition itself, such that if one were to look at the time series up to, and including the transition point, there would be no visual indication of an impending transition.

2.3.2 Observations

Autocorrelation at lag-1 and variance were calculated for the Arctic sea ice extent data using an overlapping, moving window as was done with the models. Although no official transition point was identified within the observations, because of the extreme minimum values in sea ice extent in September 2007 and 2012, the metrics were calculated using data points through March 2007. The limited length of the record only allowed the window size to be varied from 10-16 years. As with the models, the largest window size produced the most significant trend, meaning the observed metrics were found using a window size of 16 years.

2.4 Surrogate data

2.4.1 Models

To determine the likelihood of finding a trend in the metrics caused by chance, we created phase-randomized surrogate time series with the same Fourier spectrum and amplitudes as the model time series before the transitions. Applying a discrete Fast-Fourier Transform (FFT) yielded the complex power spectrum (F_k) given by,

$$F_k = \sum_{n=0}^{N-1} x_n e^{-i\,2\pi k \frac{n}{N}} \qquad k = 0, \ldots, N-1 \qquad (8)$$

The model phases were replaced by using the phase of a uniform random matrix (φ):

$$\varphi = 2\pi * X_{rand} \qquad (9)$$

where X_{rand} is a uniform matrix, the same size as the pre-transition model data set, of uniformly distributed pseudo-random numbers. The phase-randomized time series is given by,

$$X_{F_k,\varphi} = |F_k'| * \left(cos(\varphi) + i * sin(\varphi)\right) \qquad (10)$$

Using an Inverse Fast Fourier Transform (IFFT), the data in the frequency-domain is converted back to the time-domain and the surrogate time series (X_{surr}) are created

$$X_{surr} = \frac{1}{N}\sum_{k=0}^{N-1} X_{F_k,\varphi} e^{i\,2\pi k\,\frac{n}{N}} \qquad (11)$$

For each surrogate data set, the lag-1 autocorrelation and variance are computed in the same way as they were calculated for the original data. The probability that the model trend statistics would be found by chance is determined by finding the fraction of the one thousand surrogate time series which meet the following two criteria: The surrogate must meet the model change threshold, which is the pre-transition maximum lag-1 autocorrelation coefficient (variance) in the model time series minus the mean of the autocorrelation coefficients (variance) prior to the maximum point [excluding the years in which a rapid increase in autocorrelation (variance) occurred]. Second, the surrogate must have the same percent change in autocorrelation (variance), or higher, over the length of the model increase period.

2.4.2 Observations

To determine the likelihood of finding a trend in the metrics caused by chance, we also created surrogates for the observed sea ice extent time series. Observational surrogates were computed in a manner similar to the models. Even though no official transition point was identified for the observed sea ice extent time series, two fairly significant changes in sea ice extent were observed in late 2007 and 2012, so the phase-randomized surrogate time series were created with the same Fourier spectrum and amplitudes as observational record through March 2007.

The probability that the trend statistics in the observations would be found by chance was determined by finding the fraction of one thousand surrogate time series which met the following two criteria: The surrogate must meet the change threshold, which is the pre-transition maximum lag-1 autocorrelation coefficient (variance) in the observed metric minus the mean of the autocorrelation coefficients (variance) prior to the maximum point (excluding the two years of rapid increase in autocorrelation (variance)). Second, the surrogate must have the same percent change in autocorrelation (variance), or higher, for the length of the increase period in the observed metrics.

2.5 Forecast skill metric

2.5.1 Models

An analog forecast is developed and tested using the MIROC-ESM-CHEM and FIO-ESM models. A forecast period is twenty years in length with a predictor period of just under a century. For example, the first forecast period is 1961-1980, with a predictor period from 1862-1960. Using a two-month lead, the predictor period is searched for the

five nearest neighbors, or five different years in which the distance between the two months in the forecast year (x) and the two months in the predictor year (y) are minimized.

$$A_{n,m} = |(x_n - y_m)^2 + (x_{n-1} - y_{m-1})^2| \qquad (12)$$

Each year's forecast is the average of the five closest analogs from the lead month (n,m) and forward 11 months. For each year in the forecast period, this process is repeated eleven times so that each month (January through December) is used as the initiation month. Stepping the forecast and predictor periods forward one year at a time and repeating the process of selecting the five best analogs from the predictor period creates subsequent forecasts. A CLIPER (climatology + persistence) forecast is used to measure the analog forecast skill, calculated as the difference between one and the ratio of the errors in the analog and CLIPER forecasts respectively:

$$skill_{analog\ versus\ CLIPER} = 1 - \frac{analog\ error}{CLIPER\ error} \qquad (13a)$$

We also analyzed the skill of the analog forecast and a CLIPER forecast relative to climatology, calculated as the difference between one and the ratio of the errors in the analog (CLIPER) forecast and climatology:

$$skill_{analog\ versus\ climo} = 1 - \frac{analog\ error}{climatology\ error} \qquad (13b)$$

$$skill_{CLIPER\ versus\ climo} = 1 - \frac{CLIPER\ error}{climatology\ error} \qquad (13c)$$

2.5.2 Observations

An analog forecast is developed for the observations using the same process that was used for the climate models. However, given the short length of the observational record, the forecast period is seven years in length with a predictor period of just under a decade. For example, the first forecast period is 1990-1996, with a predictor period from 1980-1989. A two-month lead is used and each year's forecast is the average of the five closest analogs. This process is repeated eleven times so that each month (January through December) is used as the initiation month and the forecast is stepped forward in time through the end of the observational record. A CLIPER forecast, a more difficult forecast to beat than persistence or climatology alone, is used to measure the analog forecast skill.

3 Early warning signals

3.1 Lag-1 autocorrelation method

3.1.1 Models

An increase in lag-1 autocorrelation has been shown to be an important indicator of an impending threshold, and it has been suggested that an increase in variance is an equally important early warning metric to be used when diagnosing the threat of an impending bifurcation (Scheffer et. al 2009; Ditlevsen and Johnsen 2010). Here we analyze the change in autocorrelation and variance (measured as the standard deviation) of the MIROC-ESM-CHEM and FIO-ESM model time series to determine if the systems

slow down as their transition points are approached. Since the desire is to determine whether these metrics can be used as early warning signals for transitions in sea ice data, we did not include the actual transition point or subsequent points in our analysis.

The lag-1 autocorrelation and standard deviation were computed for both models using a sliding window of 35 years. In the ten years prior to their transitions, the MIROC-ESM-CHEM and FIO-ESM models show autocorrelation increases of 5.3% and 4.7%, and variance increases of approximately 85% and 76% respectively (Figures 7 and 8, blue and red lines; respectively). This suggests that the models systems did in fact experience dynamical slowing as they approached their respective transition points.

To test whether we would find similar results by chance, we generated one thousand phase-randomized, surrogate time series with the same Fourier spectrum and amplitudes as the portions of the original model time series used in our analysis. The probability that the model trend statistic would be found by chance was determined by the fraction of the one thousand surrogate time series, which had a similar or more impressive change in autocorrelation (variance) as the original analysis, as well as the same or better percent change in autocorrelation (variance).

The probability that an increase in lag-1 autocorrelation the same as that found in the model analysis, or better, would be observed by chance was less than 4% for both the MIROC-ESM-CHEM and FIO-ESM models. None of the surrogates yielded a variance increase equal to or better than observed for both the MIROC-ESM-CHEM and the FIO-ESM.

3.1.2 Observations

The lag-1 autocorrelation and standard deviation were computed for the observations using a sliding window of 16 years. In the two years prior to the 2007 sea ice extent minimum, the observations showed an autocorrelation increase of nearly 11% and variance increase of just over 31% (Figure 9, blue and red lines respectively). This suggests that the observed sea ice system is experiencing dynamical slowing.

Phase-randomized surrogate time series with the same Fourier spectrum and amplitudes as the observational record through March 2007 were computed as the observational surrogates. The probability that the observed trend statistic would be found by chance was determined by the fraction of the one thousand surrogate time series, which had a similar or more impressive change in autocorrelation (variance) as the original analysis, as well as the same, or better percent change in autocorrelation (variance). None of the surrogates produced changes in autocorrelation or variance that were more impressive than the observed metrics.

3.2 Forecast skill metric

3.2.1 Models

For each analog forecast, we examined three different measures of skill. In the first measure, CLIPER replaces persistence as the skill threshold, a more difficult threshold to beat than persistence or climatology alone. The skill of each analog forecast relative to climatology and that of a CLIPER forecast compared to climatology are also calculated. The skill is averaged over all forecast periods and initiation months.

The skill of the analog forecast for the MIROC-ESM-CHEM model exceeds that of a CLIPER forecast through the year 2000, for the months of April and August through December. Most notable is the marked decrease in predictability from 2012-2015, where an approximate 105% drop in skill is observed (Figure 10a; blue line). While the largest, most rapid drop in sea ice extent in the MIROC-ESM-CHEM model occurs in 2016, another significant drop in sea ice extent is observed between 2008 and 2012 (47%). Interestingly, there is another dip in skill in excess of 100% from 2000-2002, which is consistent with a forewarning of the drop in sea ice extent that begins in 2008.

We also evaluated the skill of the analog forecast and a CLIPER forecast relative to climatology. When compared to climatology, there is a roughly 24% decrease in skill for the analog forecast and just over a 37% decrease in skill for the CLIPER forecast from 1985 to 1988, a possible forewarning of the 2008 drop in sea ice extent (Figure 10b; red and blue lines respectively). The CLIPER forecast relative to climatology does not exhibit any other significant decreases in skill, but the analog forecast shows another large decrease in skill when compared to climatology. In the five years preceding the rapid loss in sea ice extent in 2016, we see a decrease in skill of nearly 10%. However, this drop is not nearly as significant as that observed in the measure of analog forecast skill computed relative to a CLIPER forecast, and given that the skill does not decrease below the values observed earlier in the record, this change in skill is a bit more difficult to argue as a warning signal.

For the FIO-ESM model, the skill of the analog forecast exceeds that of a CLIPER forecast through the year 2063 for the months of March through November. From 2058 to 2062, a 50% drop in analog forecast skill is observed (Figure 11a; blue line). We also

looked at the skill of the analog forecast and the CLIPER forecast relative to climatology to see if any warning signals were observed (Figure 11b; red and blue lines respectively). For the analog forecast skill (relative to climatology), there is roughly an 87% decrease in skill that occurs between the years 2050 and 2062. When analyzing the skill of a CLIPER forecast relative to climatology, a skill decrease of nearly 72% is observed from 2043 to 2059.

An analysis of forecast skill has shown that a decrease in predictability of the system is often expected as a transition point is approached. For the MIROC-ESM-CHEM model, a 1-6 year warning of abrupt changes in sea ice was found using a measure of analog forecast skill relative to a CLIPER forecast. For the FIO-ESM model, the analog versus CLIPER forecast skill provided a two-year warning of impending changes to the sea ice system. In examining the skill of the analog forecast and a CLIPER forecast relative to climatology, we observed similar warnings, with a possible increase in warning using the CLIPER versus climatology skill measure.

3.2.2 Observations

Analog forecasts were also created for the observations with the skill averaged over all forecast periods and initiation months. The analog forecast skill slightly exceeds that of a CLIPER forecast for the first several years, but by the year 2002 the skill of the analog forecast no longer exceeds a CLIPER forecast. Between 2004 and 2006, there is a skill drop of approximately 62% (Figure 12; blue line). This remarkable decrease in predictability is likely a forewarning of future changes to the observed sea ice system. Whether that change has already been observed or has yet to occur, remains to be seen.

4 Regional early warning signals

We examined the evolution of the sea ice extent time series at the regional scale for both the models and observations to determine whether changes were more abrupt in certain regions. We analyzed the following nine sub-regions of the total Arctic: Seas of Okhotsk and Japan, Bering Sea, Hudson Bay, Baffin Bay, Greenland Sea, Kara and Barents Seas, Arctic Ocean, Canadian Archipelago and the Gulf of St. Lawrence (not shown). Many of the sub-regions displayed decreasing trends in sea ice extent, and some even exhibited large changes in sea ice extent over a period of multiple years to decades. However, early warning signal analyses were only performed on the sub-regions in which we identified abrupt changes in sea ice extent.

4.1 Identification of distinct regions of abrupt change

The model sea ice data was processed in the same way as the analysis of the total Arctic (Equation 1): the fraction of sea ice covering each grid cell (SIC) was multiplied by the area of the grid cell (A) and weighting by the cosine of the latitude (lat) at each location. Only grid cells with greater than 15% sea ice concentration were included. The regional sea ice extent time series (extent) are the sum of all of those grid cell extent values in the areas outlined in Figures 13a and 13b.

For the MIROC-ESM-CHEM model, the Arctic Ocean exhibited the most abrupt change. The regional sea ice extent was calculated over the following areas: 125°W-105°E from 66°N-90°N, 105°E-95°W from 82°N-90°N and 95°W-125°W from 78°N-90°N (Figure 13a). For the FIO-ESM model, the region of most abrupt change was

found in the Greenland Sea and is defined by the following areas: 15°E-0°E from 70°N-90°N, 0°E-10°W from 66°N-82°N, 10°W-30°W from 55°N-82°N and 30°W-45°W from 50°N-70°N (Figure 13b).

The MIROC-ESM-CHEM surface air temperatures and sea ice extent for the Arctic Ocean region from 1861-2100 for the month of September are displayed in Figure 14. This model exhibits a significant rise in surface temperatures across the Arctic Ocean region and a rapid loss of sea ice, with all but a few of the Septembers after 2050 being virtually, if not completely, ice free. Between 2009 and 2012, the sea ice extent in the Arctic Ocean drops by over 15%, and a threshold is reached in 2015 that shifts the system to a contrasting state. Sea ice extent sharply declines during the subsequent four years, exhibiting a change in the Arctic Ocean's average September sea ice extent of roughly 84% (catastrophic bifurcation; Scheffer et. al 2009).

As shown in Figure 15, during the month of March, the Greenland Sea region in the FIO-ESM model exhibits cooling in the latter part of the 21st century and a rise in sea ice extent beginning just prior to 2050, with new maximum sea ice extent values reached near the end of the record. In contrast to the MIROC-ESM-CHEM model, the FIO-ESM model sea ice values remain relatively stable until the year 2045, when there sea ice extent rises to a value roughly 28% higher than the sea ice extent two years prior. The sea ice extent displays a steady upward trend until the year 2065, when it exhibits an abrupt increase. In just three years, this model displays a nearly 40% increase in the average sea ice extent over the Greenland Sea, peaking at nearly 256% above the mean sea ice extent prior to the year 2045.

The observed surface air temperature for the month of September over the Arctic Ocean exhibits a subtle increasing trend at the end of the record, and the amplitude of the year-to-year fluctuations increases (Figure 16; grey line). The black line in Figure 16 shows that the observed sea ice extent for September over the Arctic Ocean is very similar to that shown in Figure 6 (black line) for the total Arctic. The observed September sea ice extent over the Arctic Ocean displays two abrupt drops, with new minimums observed in 2007 and 2012. The 2007 minimum is just over four standard deviations below the mean sea ice extent observed through the year 2006, with the 2012 minimum approximately five standard deviations below the mean sea ice extent through 2006.

4.2 Lag-1 autocorrelation method: Regional analysis

4.2.1 Models

The lag-1 autocorrelation and standard deviation were computed for both regional model time series using a sliding window of 35 years. The actual transition point or subsequent points were not included in our analysis. The MIROC-ESM-CHEM regional model time series abruptly shifts to a near ice-free state in the year 2015. In the seven and a half years prior to its transition, the MIROC-ESM-CHEM model shows an autocorrelation increase of 7.5% and a variance increase of nearly 37% (Figure 17; blue and red lines, respectively). An autocorrelation increase of nearly 6% and a variance increase of just over 31% are observed in the ten and a half years prior to the 2065 abrupt shift in the FIO-ESM regional model time series (Figure 18; blue and red lines,

respectively). This suggests that the model's sea ice subsystems did in fact experience dynamical slowing as they approached their respective transition points.

To test whether we would find similar results by chance, we generated one thousand phase-randomized, surrogate time series with the same Fourier spectrum and amplitudes as the portions of the original model time series used in our regional analysis. The probability that the model trend statistic would be found by chance was determined by the fraction of the one thousand surrogate time series, which had similar or more impressive changes in autocorrelation (variance) as the original analysis, as well as the same or better percent change in autocorrelation (variance).

The probability that an increase in lag-1 autocorrelation the same as that found in the regional model analysis, or better, would be observed by chance was less than 2% for the MIROC-ESM-CHEM and around 0.1% for the FIO-ESM models. None of the surrogates yielded a variance increase equal to or better than observed for both the MIROC-ESM-CHEM and the FIO-ESM.

4.2.2 Observations

The time series of observed Arctic Ocean sea ice extent anomalies is displayed in Figure 19. A clear phase shift occurs near the end of the record and the 2007 and 2012 September minimums are clear as well. The lag-1 autocorrelation and standard deviation were computed for the regional observed time series using a sliding window of 16 years. The actual transition point or subsequent points we not included in our analysis. In the two months prior to the September 2007 sea ice minimum, the autocorrelation increased

by 17%, with a variance increase of 23%. None of the surrogates yielded an autocorrelation or variance increase equal to or better than observed.

4.3 Forecast skill metric: Regional analysis

4.3.1 Models

As was done in the analysis of the total Arctic, the analog forecast period is twenty years in length, but the first forecast period for the regional analysis is 1931-1950, with a predictor period from 1862-1930. We examined three different measures of skill: analog forecast versus a CLIPER forecast, analog forecast versus climatology and CLIPER versus climatology. The skill was averaged over all forecast periods and initiation months. However, it was determined that while the sea ice extent in the Arctic Ocean region of the MIROC-ESM-CHEM model exhibited a significant and rapid decline to ice-free or nearly ice-free during the months of August through October, the remaining months show little change in the overall monthly mean sea ice extent (though large, short-term deviations are observed). This enormous increase in the seasonal cycle resulted in a very poor persistence forecast for most of the months examined. Therefore, any discussions of forecast skill in the regional analysis for the models refer to the analog forecast compared to a climatological forecast.

The September sea ice extent over the Arctic Ocean for the MIROC-ESM-CHEM model and the analog forecast skill are displayed in Figure 20a. The sea ice extent time series for the Arctic Ocean is markedly similar to that for the total Arctic. There is a rapid decline in sea ice extent that begins in 2015, with an 84% decrease in sea ice extent by September 2019. The forecast skill for this month exhibits a decrease of more than

200% from 1965 to 1971, possibly forewarning of the rapid shift in 2015. The forecast skill then displays an increasing trend for roughly the next 45 years, with a smaller drop in skill in 2018.

Even though the mean sea ice extent during the winter months showed very little change during the 1861 to 2100 period, there were significant deviations from the mean. The February sea ice extent and analog forecast skill for the Arctic Ocean region of the MIROC-ESM-CHEM model are displayed in Figure 20b. There is a less than 1% change in the mean sea ice extent over the 1861 to 2100 time period, but there are two extreme minima observed in 2027 and 2054, with nearly 1.5% and 3.5% decreases over periods of one and two years, respectively. The forecast skill also exhibits two notable decreases. The first occurs from 1968-1972 when a nearly 19% drop in skill is observed. An almost 32% skill decrease is found between 2019 and 2023.

The March sea ice extent over the Greenland Sea for the FIO-ESM model and the analog forecast skill are displayed in Figure 21. The time series of Greenland Sea ice extent is quite similar to the sea ice extent time series for the total Arctic. The sea ice extent over the Greenland Sea first shows an increase in 2040, with a nearly 30% increase in just one year. The sea ice extent continues to increase steadily until 2065, when the average March sea ice extent increases by almost 40% in just three years, an increase of more than 2.3 million square kilometers above the mean sea ice extent prior to 2040. The analog forecast skill decreases by almost 34% from 1995 to 1998, with a decrease in predictability of nearly 76% from 2037 to 2057.

The regional analysis of forecast skill has shown that the anticipated decrease in predictability of a system as it approaches a transition point is detectable at the regional

level. In fact, it has been shown that the regional analysis provides a much earlier warning of future sea ice changes within the climate models.

4.3.2 Observations

The analog forecast for the Arctic Ocean is developed using a seven year forecast period (1990-1996), with a predictor period of just under a decade (1980-1989). A two-month lead is used and each year's forecast is the average of the five closest analogs. A CLIPER forecast is used to measure analog forecast skill.

The September sea ice extent over the Arctic Ocean for the observations and the analog forecast skill are displayed in Figure 22. The sea ice extent time series for the Arctic Ocean shows a much weaker decreasing trend in sea ice extent prior to the year 2000 than was seen in the total Arctic time series. The sea ice extent rapidly declines after that point, with the sea ice extent falling more than 2 $mil.km^2$ below the long term mean in 2007, and declining 27% more by 2012.

The analog forecast skill also declines rapidly, with a 107% decrease from 2004 to 2006. The skill becomes positive again from 2008-2010, dropping by 95% from 2010 to 2011. Our regional forecast skill analysis shows there was a significant decrease in predictability in the observed sea ice system by 2006, perhaps forewarning of the 2007 minimum, or signifying a more drastic shift that has yet to be seen.

5 Stochastic sea ice model

A mathematical model developed by EW09 reduces the intricacies of the Arctic sea ice system to an ordinary differential equation forced by the observed Arctic seasonal cycle. Their model produced a simulation of the Arctic sea ice seasonal cycle that is consistent with observations, providing insight into the qualitative behavior of the Arctic sea ice system. Using the methods outlined in EW09, we create a stochastically forced single column model, which describes the evolution of the temperature profile of the ocean mixed layer in the Arctic. A model schematic is shown in Figure 23.

A single column model is used to determine the energy per unit area of the system (E). To account for ice thickness when ice is present and the temperature of the ocean mixed layer when ice is absent, the variable E is defined as:

$$E \equiv \begin{cases} -L_i h_i & E < 0 \\ c_{ml} H_{ml} T_{ml} & E \geq 0 \end{cases}, \tag{14}$$

where L_i is the latent heat of fusion for sea ice, h_i is sea ice thickness, c_{ml} is the specific heat capacity of the mixed layer, H_{ml} is the depth of the mixed layer, and T_{ml} is the temperature of the ocean mixed layer (relative to the freezing point). Together this accounts for the ice thickness when ice is present and the temperature of the ocean mixed layer when the ocean is ice-free.

Assuming heat flux balance at the top of the atmosphere, the rate of change of E with respect to time is proportional to the net energy flux,

$$\frac{dE}{dt} = \overbrace{[1-\alpha(E)]\,F_s(t)}^{Shortwave\ forcing} - \overbrace{[F_0(t) + F_T(t)\,T(t,E)]}^{Longwave\ forcing} + \overbrace{\Delta F_0}^{External\ forcing}$$

$$+ \overbrace{F_B}^{Ocean\ heating} + \overbrace{v_0\,R(-E)}^{Ice\ transport} \qquad (15)$$

The top of the atmosphere net solar radiation fluxes are represented by $[1-\alpha(E)]\,F_s(t)$, where $F_s(t)$ is the incident shortwave radiative flux at the surface and varies seasonally. The outgoing longwave radiation term includes $F_0(t)$ and $F_T(t)$, which are atmospheric model derived quantities that include clouds, air temperature south of the Arctic and atmospheric transport into the Arctic (seasonally-derived). The terms $F_s(t), F_0(t)$ and $F_T(t)$ are defined according to observed values in the central Arctic (see Table 1). The term F_{south} in Figure 23 represents the atmospheric transport into the Arctic and is incorporated into the model through the derivations of the parameters $F_0(t)$ and $F_T(t)$. Assuming that energy associated with phase changes exceeds that for temperature changes, the vertical diffusion equation yields a linear temperature profile and the ocean heat flux into the bottom of the ocean mixed layer or sea ice is defined as $\frac{k_i}{h_i}(T_{ml})$, where the constant k_i is the ice thermal conductivity and is derived from observations. This causes thin ice to grow faster than thick ice. Warming in the model is set by ΔF_0, the surface heat flux. The term v_0 represents ice export out of the Arctic (when ice is present). The ramp function, $R(x)$ is defined as:

$$R(x) = \begin{cases} x & when\ x \geq 0 \\ 0 & when\ x < 0 \end{cases} \qquad (16)$$

and ensures that v_0 is zero when sea ice is absent.

When the average energy of the Arctic (E) is near zero, there will likely be both ice covered and ice free regions. When E increases through zero, a smooth transition from an ice-covered to ice-free ocean is achieved by varying the model's top of the atmosphere albedo between the values for ice (α_i) and ocean mixed layer (α_{ml}), using the thickness parameter h_α. Specifically,

$$\alpha(E) = \frac{\alpha_{ml} + \alpha_i}{2} + \frac{\alpha_{ml} - \alpha_i}{2} \tanh\left(\frac{E}{L_i h_\alpha}\right). \qquad (17)$$

When ice is present ($E < 0$), the surface temperature is calculated from the surface energy balance between the upward heat flux in the ice and the energy flux above it. When the surface temperature warms to the freezing point and melting occurs ($E = 0$), $T(t, E)$ is set to zero. If no sea ice is present ($E > 0$), the ocean mixed layer is represented as a thermodynamic reservoir using equation 14. The above cases are combined here:

$$T(t,E) = \begin{cases} -R\left[\dfrac{(1-\alpha_i)\,F_s(t) - F_0(t) + \Delta F_0}{\dfrac{k_i L_i}{E} - F_T(t)}\right] & E < 0 \\ \dfrac{E}{c_{ml} H_{ml}} & E \geq 0 \end{cases} \qquad (18)$$

A predictor-corrector method is used to solve the ordinary differential equation, with the predictor defined as:

$$E_{j+1} = E_j + \Delta t\left(\left.\frac{dE}{dt}\right|_j + \frac{S}{\sqrt{\Delta t}}\right), \qquad where\ S \equiv stochastic\ forcing \qquad (19a)$$

and the corrector step:

$$E_{j+1} = \frac{1}{2}\left(E_{j+1} + E_j + \Delta t\left(\left.\frac{dE}{dt}\right|_{j+1} + \frac{S}{\sqrt{\Delta t}}\right)\right) \qquad (19b)$$

The idealized Arctic sea ice-ocean atmosphere model developed by EW09 was re-created here used to investigate the behavior and predictability of sea ice within the model when bifurcation behavior is observed. We used the same values for the parameters as defined in EW09 and they are displayed in Table 1. We varied the imposed surface heat flux (ΔF_0) as well as the level of stochastic forcing (S) until we observed bifurcation behavior within the model. The model output E represents the ocean temperature in degrees Celsius (T_{ml}) when $E > 0$ and the sea ice thickness in meters (h_i) when $E < 0$ (using Equation 14):

$$h_i = \frac{E}{-L_i} \qquad E < 0 \quad (sea\ ice) \qquad (20)$$

$$T_{ml} = \frac{E}{c_{ml}H_{ml}} \qquad E \geq 0 \quad (ocean) \qquad (21)$$

An early warning signal analysis was performed on the model realizations that exhibited bifurcation behavior to determine whether our warning metrics are detectable in this simplified model.

5.1 Model results

Using their sea ice ocean atmosphere model that produces a simulation of the Arctic sea ice seasonal cycle that is consistent with observations, EW09 investigated the physical mechanisms behind potential bifurcation behavior in the Arctic sea ice system. They argue that as greenhouse gas levels increase, the transition from perennial to seasonal ice cover will be a smooth transition, and that an abrupt transition to perennially ice-free conditions can only be achieved when greenhouse gases are increased further.

In a more recent study, Abbot et al. (2011) utilize a similar low-order sea ice model, but include additional physical effects such as changes in clouds and heat transport as sea ice retreats, arguing that these additions avoid issues that might arise from the use of observations that represent an Arctic that is ice-covered year round. Though they find a larger range of bifurcation behaviors, they agree with the findings of EW09; bifurcation behavior is more likely to be observed during winter-only sea ice conditions.

Figure 24 is a diagram of solutions to EW09's model (Eisenman and Wettlaufer 2009; Figure 3) and shows how the inclusion of non-linear sea ice thermodynamic effects alters the model results when compared to a partially linearized model that represents the Arctic Ocean as a thermal reservoir with a temperature dependent albedo (Eisenman and Wettlaufer 2009; Hartmann 1994). For each value of the imposed surface flux ΔF_o, the model is run until is converges on a steady-state seasonal cycle and the annual maximum and minimum values of E are plotted (right axis on Figure 24). The corresponding sea

ice thickness in meters (h_i) or ocean mixed layer temperature in °C (T_{ml}) are plotted on the left axis of Figure 24.

The full non-linear model exhibits a smooth transition from a perennially ice-covered ocean (Figure 24; blue lines) to a state of seasonal sea ice when sea ice is present during a large fraction of the year (Figure 24; red lines). Further warming within the model causes a bifurcation and the loss of the remaining seasonal (winter) ice cover. The grey lines in Figure 24 represent the post transition period, with perennially ice-free conditions that are irreversible. The value of ΔF_o at which a transition occurs depends on the choices of the model parameters, but the qualitative features of Figure 24 are robust (Eisenman and Wettlaufer 2009).

The model exhibits strong sea-ice thermodynamic effects that help to stabilize the model, particularly when ice is present during a large portion of the year. Once the model transitions to seasonally ice-free conditions, the heat flux increases and the ice albedo feedback results in an increased warming rate (notice difference in slopes of blue and red curves in Figure 24). This causes the ice-covered fraction of the year to decrease as the climate warms, eventually reaching a point where ice cover is present during only a relatively small portion of the year and the ice albedo feedback dominates, resulting in a bifurcation (perennially ice-free conditions).

Figures 25 (a-d) display the range of solutions produced by the model when it is run for one hundred years with the imposed surface heat flux (ΔF_o) set to $22.25\ Wm^{-2}$. The stochastic forcing level (S) and initial energy ($E(1,1)$) are varied. With the stochastic forcing and the initial energy set to $0\ Wm^{-2}$, the model is in a seasonally ice-free state with an ice-covered ocean during a large fraction of the year (Figure 25a). No

transition to ice-free conditions occurred during this simulation. When the initial energy is set to 30 Wm^{-2}, the model immediately transitions to perennially ice-free conditions (Figure 25b). Reducing the initial energy value to 13 Wm^{-2} but turning on the stochastic forcing to a level of 1 Wm^{-2}, results in a solution where seasonally ice free conditions are observed for a very short time out of the year and as the model climate warms, the ice-covered fraction of the year diminishes until the system suddenly transitions to perennially ice free conditions. However, this transition occurs at different points within each model run (Figures 25c and 25d).

5.2 Lag-1 autocorrelation method

The model is run with a nearly 200-year spin-up period and the resulting sea ice time series is the same length as the climate model time series. The surface heat flux (ΔF_0) is set to 22.25 Wm^{-2} with stochastic forcing set to 1.05 Wm^{-2}. With these parameter values the model produces a range of solutions, with some realizations producing a seasonally ice-free Arctic and others transitioning rapidly to an ice-free state. We collected ten runs, which experienced a rapid transition to an ice-free state and centered them on their transition points, retaining roughly twenty years before and after the transition point. Then we performed an early warning signal analysis on the centered time series.

The autocorrelation and variance (measured as the standard deviation) were calculated in the same manner as our previous analyses, with a window size of seven years due to the short record length of just forty years. The average of the ten time series are shown in Figure 26a and 26b. The grey line shows the rapid increase in E, beginning

at the transition point (marked by the vertical black line). In a ten-year period, E increases by 184%. Three years before this transition, the autocorrelation exhibits an increase of 15% over a two-year period (Figure 26a; blue line). The variance, measured as the standard deviation, increases by 24.5% in two years and this change occurs three years prior to the transition point (Figure 26b; red line). Using our stochastic sea ice model we have shown that a rapid transition to ice free conditions occurs for certain model parameters and we are able to detect autocorrelation and variance increases ahead of the transition, providing a roughly three-year warning of the impending change.

To examine the false alarm rate produced by the autocorrelation and variance method, we produced one hundred simulations using the sea ice model in a stable state. Specifically, we turned down the surface flux (ΔF_o) to 15 Wm^{-2}, but kept the stochastic forcing level the same. To test whether the increase in the metrics was noteworthy, we computed autocorrelation and variance metrics for each of the one hundred stable simulations from our ice model. We found the maximum value for each metric and determined how many standard deviations it was above the mean prior to that point. We also computed the change between the maximum in the metrics and the value two years prior (consistent with the results from the transition time series in Figures 26a and 26b). If the maximum in the autocorrelation and variance metrics for the stable time series were more than three standard deviations above the mean prior to that point and the change in the metrics exceeded that observed in our transition case, then we considered the case a false alarm. The false alarm rate for this early warning method was 8%.

5.3 Forecast skill metric

For the forecast skill analysis we looked at the error in the analog forecast relative to climatology. We used an average of the ten transition simulations above, but retained the seventy years before and approximately thirty years after the transition, yielding a time series of roughly one hundred years for the forecast skill analysis. A forecast period is twenty years in length with a predictor period of just under thirty years. The skill measure is displayed in Figure 27 (red line) shows a 93% drop in skill from years 60-66. The drop in predictability occurs four years prior to the transition point (year 70), providing a forewarning of the rapid change within the model.

To examine the false alarm rate produced by our analog forecast method, we used the same one hundred simulations of the sea ice model in a stable state that were used for the autocorrelation and variance analysis. An analog forecast is computed for each time series and the skill against climatology is determined. To test whether a decrease in skill was noteworthy, we searched each skill vector for the minimum value and determined how many standard deviations it was below the mean prior to that point. We also computed the change in the skill between the minimum and seven years prior (consistent with the results from the transition time series in Figure 27). If the minimum skill value was more than three standard deviations below the mean prior to that point and the change in skill exceeded that observed in our transition case, then we considered the case a false alarm. The false alarm rate for this method was 24%, which is worse than the autocorrelation and variance metric, but is still far better than the false alarm rates typically observed for tornado warnings and on the lower end of the range for precipitation forecasts (Barnes et al., 2007; McBride and Ebert, 2000).

6 Sea ice albedo feedback as a driver of abrupt change

We demonstrated a set of metrics to be used for warning of bifurcations within two global climate models and have shown that these metrics are applicable to a simplified stochastic sea ice model. Furthermore, our results show that the sea ice exhibits predictability on seasonal time scales when bifurcation behavior is not observed, which is consistent with previous studies (Juricke et al., 2014). But truly meaningful predictions of Arctic sea ice continue to be limited by our understanding of the physical mechanisms forcing abrupt changes within the Arctic system (Bekryaev et al., 2010). Given the substantial range in model projections of the future Arctic climate and the role of the Arctic in global climate change, determining what is causing these differences in simulated Arctic climate is crucial (Boe et al., 2009).

Changes to sea ice extent are likely due to a combination of natural and anthropogenic variability in the ocean-atmosphere system. Sea ice extent changes can be thermodynamic, due to changes in surface air temperature or radiative fluxes, or dynamic, resulting from modifications to the ice circulation in response to winds and ocean currents (Bekryaev et al., 2010; Stroeve et al., 2011). However, the relative contributions of these different processes are debated.

Often cited as the strongest contributor to high latitude climate change, and more importantly accelerated changes, is the sea ice albedo feedback (SIAF); the reduction of snow and ice due to anthropogenic induced warming leads to more open land and water, which decreases the albedo and increases solar absorption, inducing a further increase in temperature (Holland and Bitz, 2003; Hall 2003; Curry and Schramm 1994; Manabe and Stouffer, 1980). More recent studies have proposed that longwave radiation effects play

an equal or even greater role in Arctic amplification than the SIAF (Winton, 2006; Graversen and Wang 2009). On the other hand, it has also been suggested through heat budget estimates that SIAF mechanisms cannot alone explain the recent surface air temperature anomalies or reductions in Arctic sea ice extent (Bekryaev et al., 2010). Discussions of dynamic causes of Arctic sea ice loss are more limited, but several studies have shown that ice transport out of the Arctic can be enhanced by winds and sea ice drift associated with sea level pressure anomalies. In fact, a recent study revealed that nearly 30% of the recent Arctic sea ice loss could be attributed to summer atmospheric circulation patterns (Timmermans et al., 2009; Ogi et al., 2008).

To determine what is driving these changes in the modeled Arctic climate, we estimated the surface (column) albedo for each model period by calculating the ratio of upward to downward reflected shortwave radiation at the surface (top of the atmosphere) (Figures 28a and 28b). The two models, which produce vastly different sea ice scenarios in the 21st century, show little variation in albedo trends prior to the year 2000. The average surface (column) albedo difference between the two models peaks at 0.15 (0.08), with a mean difference of roughly 0.04 (0.01), depending on the month of the year. Furthermore, there are no significant changes in albedo that would warrant the substantial changes in sea ice produced by each model. In the 10 years prior to the MIROC-ESM-CHEM model collapse (2006 to 2015), the difference in surface (column) albedo peaks just below 0.1 (< 0.07), with an average difference of just under 0.03 (< 0.02).

In addition to an average model difference in surface (column) albedo of approximately 0.03 (< 0.02) in the years prior to the MIROC-ESM-CHEM model's collapse (2016), there is no sudden change in albedo in the MIROC-ESM-CHEM model

(FIO-ESM model) prior its collapse (recovery), effectively excluding sea ice albedo feedback as the driving force of drastic sea ice changes within these models. Instead, it appears to be a feedback with a strength that is a strong function of the model's Arctic low cloud and boundary layer parameterizations. The fact that such disparate behavior in these clouds can be found in these two models is disconcerting, hinting at the difficulty in capturing even a bulk description of climate response to sea ice variability.

7 Discussion and Conclusions

We have shown that lag-1 autocorrelation and variance can be used as early warning signals of impending transitions in two global climate models and observations, for the full Arctic region as well as sub-regionally, and for a simple stochastic sea ice model. Slowing down was detectable prior to the transitions, as evidenced by the significant rise in the metrics ahead of the transition points. Additionally, we created an analog forecast, which demonstrated skill over a climatological forecast, and in some cases a CLIPER forecast.

For the MIROC-ESM-CHEM and FIO-ESM model, the warning varied between 7.5 and 10.5 years for the autocorrelation and variance metrics. Depending on the skill metric used, the warning time for the climate models ranged from 1 year to roughly 20 years for the full Arctic region, with the length of warning increasing at the regional level.

Determining the amount of forewarning provided in the observational analyses is difficult since we don't know whether they are predictions of the recent extreme reductions in sea ice or ones yet to be observed. For the purpose of discussion, we will

assume they are warning signals for the most recent abrupt reductions to summer Arctic sea ice extent (2007 minimum). The current length of the observational sea ice record required reducing the 35-year window used in the model analysis to 16 years. However, we were still able to identify clear warning metrics using the observed sea ice extent data, implying that the window size of 16 years was sufficient enough that we can effectively rule out the possibility of a false positive (Knutti and Stocker 2002). This was also confirmed by our surrogate analysis.

The autocorrelation and variance metrics provided an approximate two-year warning, with the measure of skill providing a forewarning of one year for the observational data covering the entire Arctic. When the analysis was performed regionally, the autocorrelation and variance metrics provided a two-year warning of impending sea ice changes over the Arctic Ocean region, and a two-month warning was provided using the skill metric. So while the reliability of future sea ice predictions would likely decrease as we near a threshold, it may be possible to identify an approaching sea ice threshold in observations.

It was determined that the early warning metrics were detectable in realizations of a stochastic sea ice model as it transitioned from seasonal sea ice conditions to a perennially ice free state. The autocorrelation and variance metrics provided a three-year warning, with the forecast skill metric warning of the impending regime shift four years before the event. The false alarm rates for these metrics were found to range from 8% to 24%, respectively, suggesting that the autocorrelation and variance metric is more reliable than the forecast skill method, though the latter provided a slightly earlier warning.

The forecast skill metric combined with the lag-1 autocorrelation and variance method provides us with a robust set of warning signals for abrupt changes to the sea ice system. Although these metrics may help to warn of an impending transition, the actual moment of a transition remains difficult to predict, and our statistics do not provide insight into the geo-physical mechanisms driving these abrupt changes. So while these early-warning signals may be a large step forward in our ability to say whether the probability of a bifurcation event is increasing, improving our understanding of the underlying physical mechanisms determining their behavior is crucial to improving sea ice forecasts, particularly near bifurcation points (Scheffer et. al 2009).

While an ultimate goal to improve sea ice forecasts is warranted, given that Arctic sea-ice has been labeled as one element of Earth's climate system that is under the greatest threat for reaching a tipping point, it is also imperative that we invest time and energy into mitigation and adaptation strategies for a shift in the Arctic sea ice system. The length of warning provided by the metrics discussed here suggests we might have the ability to respond and take action. While a tipping point may not be preventable, measures could be taken to lessen the impact resulting from a given transition (Lenton 2012).

Should the amount of forewarning in the observations turn out to be similar to that of the models analyzed here, then curbing emissions of long-lived CO_2 *might* have some effect on moderating the impact of an Arctic sea ice transition, *if* a global response can be initiated. However, given the length of the anticipated warning period and the unlikelihood of a global response, a better approach might be to limit other pollutants that impact sea ice, such as methane, tropospheric ozone and black carbon, all of which have

shorter lifespans in the atmosphere and would result in a quicker reduction in radiative forcing (Lenton 2012).

8 Future work

Multiple studies have investigated the bifurcation structure of sea ice loss using single column models, resulting in a broad range of scenarios, including both smooth and abrupt transitions between perennial sea ice and seasonal sea ice and between a seasonally ice covered and a seasonally ice free Arctic. In a recent comprehensive study, a toy model was used to demonstrate that all of the above scenarios were possible by varying the parameters within the model. The results were used to interpret the differences in the sea ice projections produced by two global climate models, showing that a low-order sea ice model is beneficial for a conceptual understanding of the sea ice system (Eisenman, 2012).

The two global climate models analyzed here exhibit only minor differences in albedo, despite their vastly different sea ice evolutions, suggesting the extreme sea ice changes within the models are not temperature dependent. This leaves the possibility that a dynamic event is responsible for the drastic changes observed within the models. Pressure anomalies are capable of modifying wind patterns to cause deformation of the ice, thus creating thicker, longer-lasting ice (recovery). Alternatively, an altered wind pattern may favor ice transport out of the Arctic, therefore enhancing ice loss (collapse). The representations of dynamic processes such as ice transport out of the Arctic could be investigated as causes for the stark differences in the MIROC-ESM-CHEM and FIO-ESM model sea ice evolution (Eisenman 2012; Kattsov et al. 2010).

In addition, the only parameters that were varied in our analysis of the stochastic sea ice model were the imposed surface heat flux, the initial value of E and the level of stochastic forcing (ΔF_o , $E(1,1)$ and S). In the current study, the albedo values for when the ocean is ice-free (α_{ml}) and ice-covered (α_i) were set to 0.2 and 0.68 as specified in EW09. It would be beneficial to reassign these values based on our global climate model results. Changing these parameters would likely affect the level of surface forcing (ΔF_o) necessary for bifurcation behavior within the models. If we could alter the stochastic sea ice model to reproduce the results of the MIROC-ESM-CHEM and FIO-ESM models it may help determine the parameters that cause such diverse behavior within these two climate models.

For example, Eisenman (2012) finds that increasing the seasonal time lag between shortwave and longwave forcing components in his model causes a decrease in the amplitude of the total forcing, eventually reaching the point where the two forcings are completely out of phase with one another and sea ice growth is limitless. This is the only scenario in which the sea ice grows and is comparable to the FIO-ESM model analyzed in our study. In addition, the EW09 model does not include modifications in cloud cover associated with sea ice changes nor does it alter ocean heat transport as sea ice is lost, both of which could significantly alter the model climate and allow for bifurcation behavior when shifting from perennial to seasonal sea ice as we observed in the MIROC-ESM-CHEM model (Abott et al. 2011). Therefore, an investigation into the differences between these parameters in the FIO-ESM model and the MIROC-ESM-CHEM model might further our understanding of their vastly different projections of future Arctic sea ice.

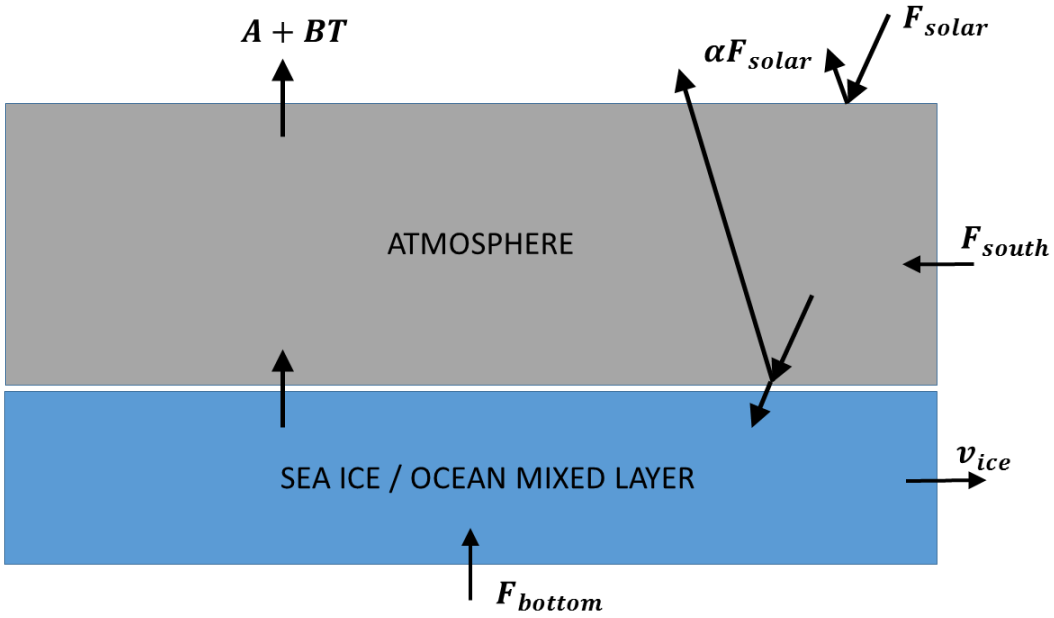

Figure 1. Schematic of the thermodynamic and dynamic (v_{ice}) components of the sea ice ocean atmosphere system.

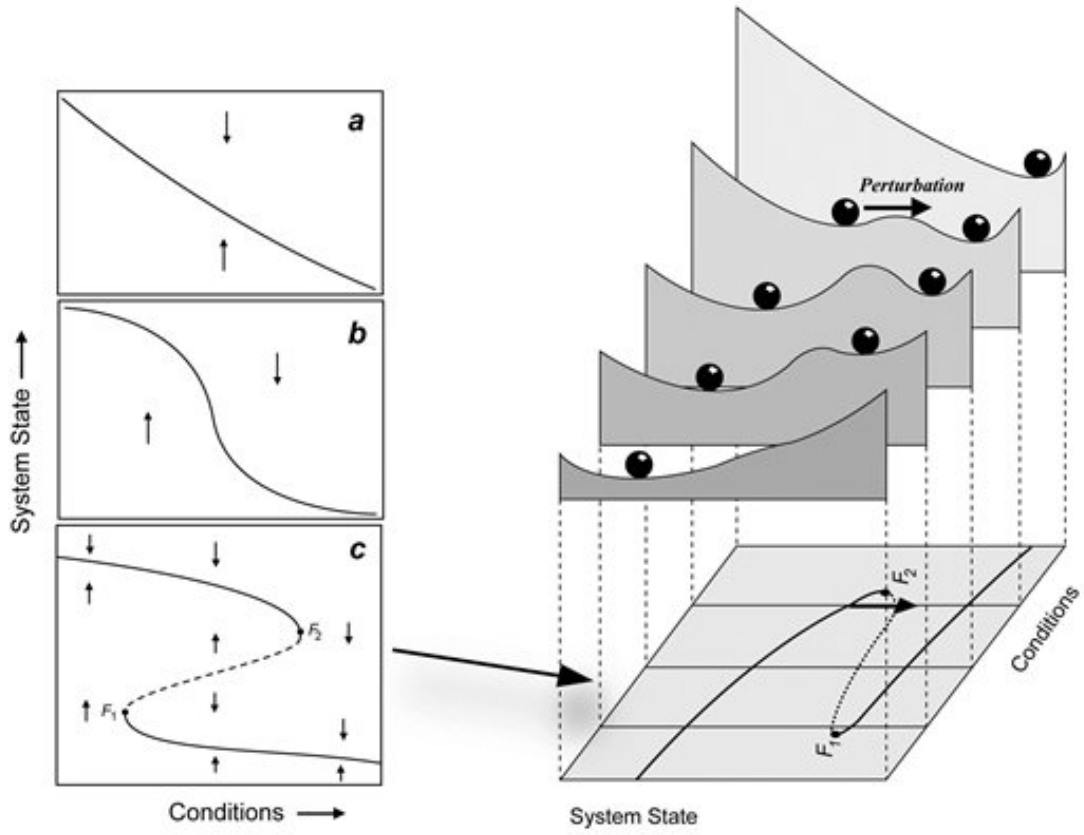

Figure 2. Schematic of system response to small perturbations. A small change in forcing usually results a smooth, gradual and reversible response to the system. In case (b), small changes in forcing result in disproportionately large changes to the system, but remain reversible. In panel (c), small changes have resulted in an abrupt shift in the state of the system (critical transition). The right panel shows how small perturbations to the system can appear to have no effect, until the system nears the tipping point. The resilience of the system decreases (basin of attraction shrinks) until the point where even a tiny perturbation causes a critical transition. Figure is borrowed from the following website: http://www.early-warning-signals.org/theory/what-is-a-critical-transition/ and was developed by SparcS Center (Scheffer et al. 2015).

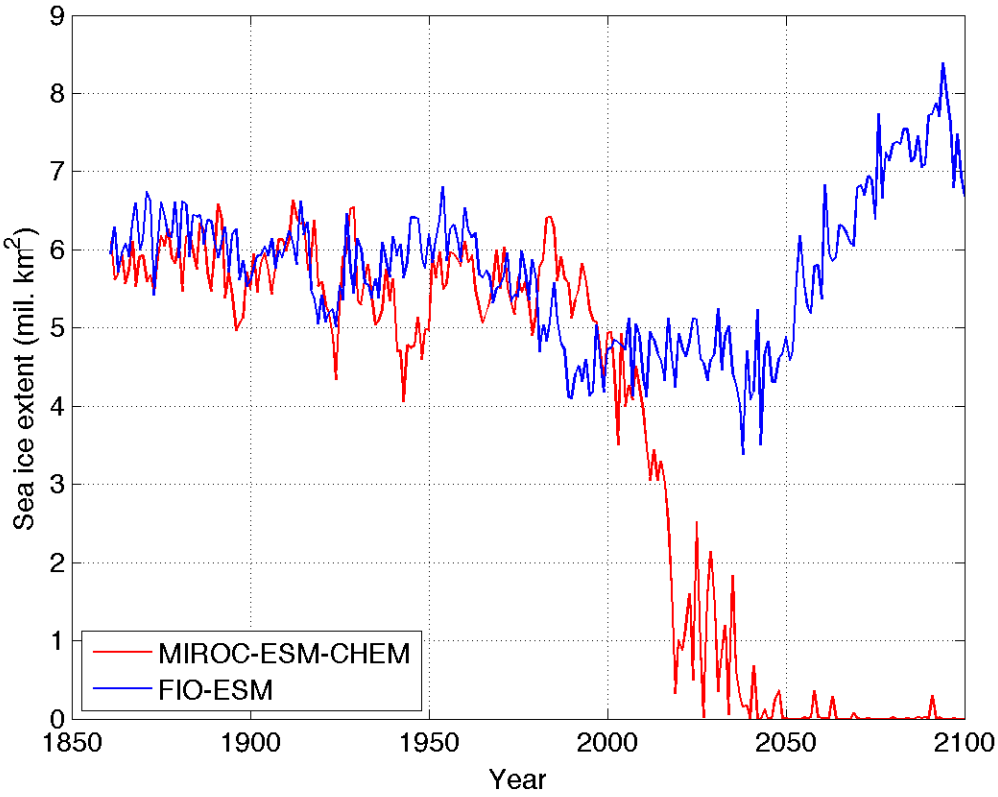

Figure 3. September sea ice extent ($mil.km^2$) averaged over 40°N to 90°N for the MIROC-ESM-CHEM (red) and FIO-ESM (blue) models for the period 1861-2100.

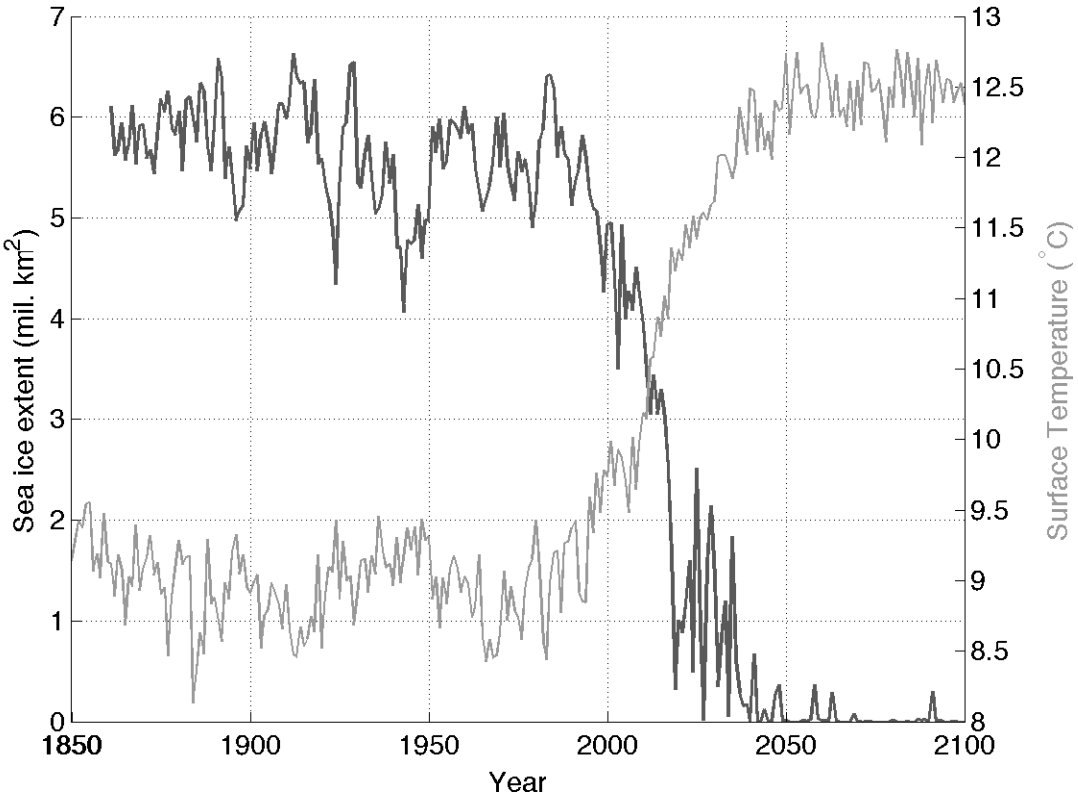

Figure 4. Sea ice extent ($mil.km^2$) and surface temperature (°C) averaged over 40°N to 90°N for the MIROC-ESM-CHEM model for September from 1861-2100 and 1850-2100 respectively.

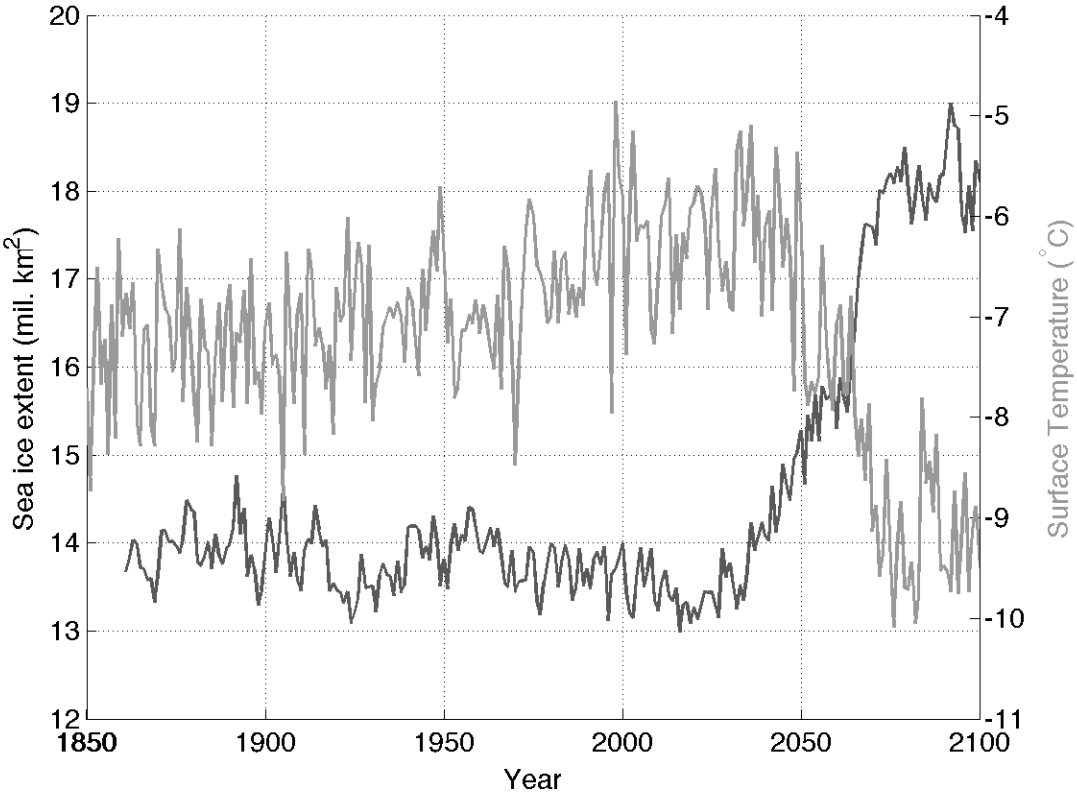

Figure 5. Sea ice extent ($mil.km^2$) and surface temperature (°C) averaged over 40°N to 90°N for the FIO-ESM model for March from 1861-2100 and 1850-2100 respectively.

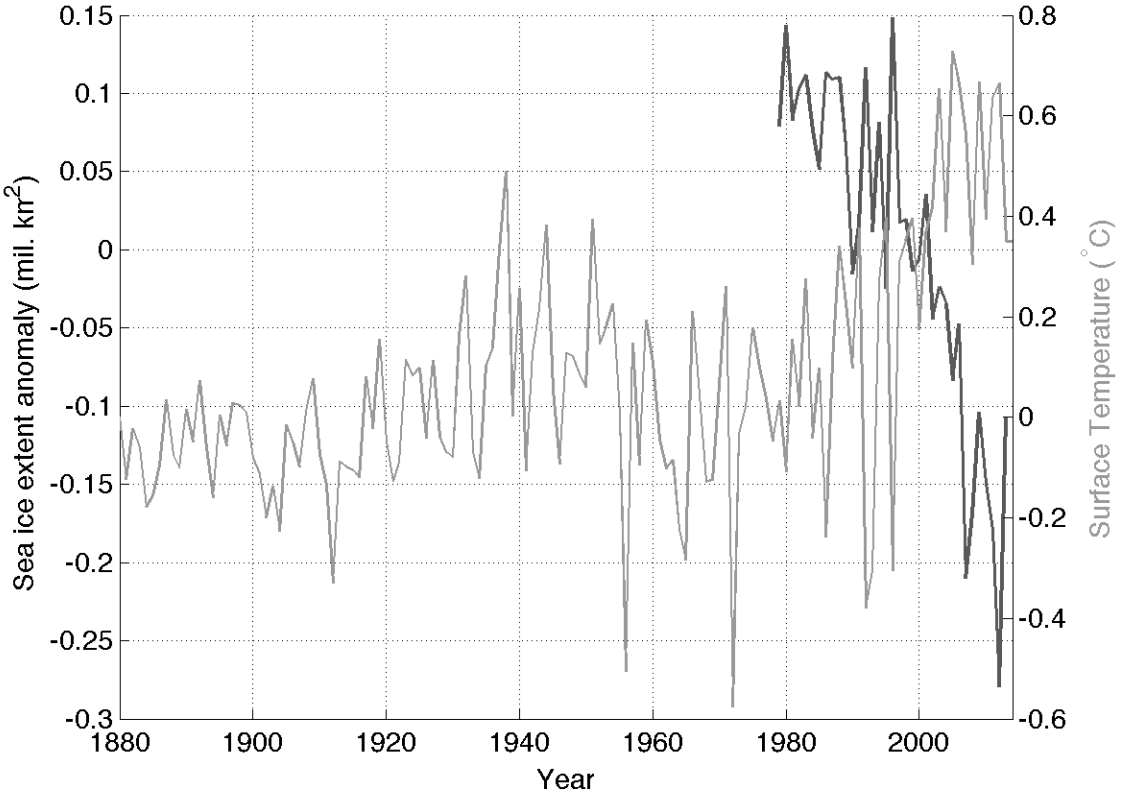

Figure 6. Observed sea ice extent anomaly and surface temperature anomaly (°C) averaged over 40°N to 90°N for September from 1979-2013 and 1880-2014 respectively.

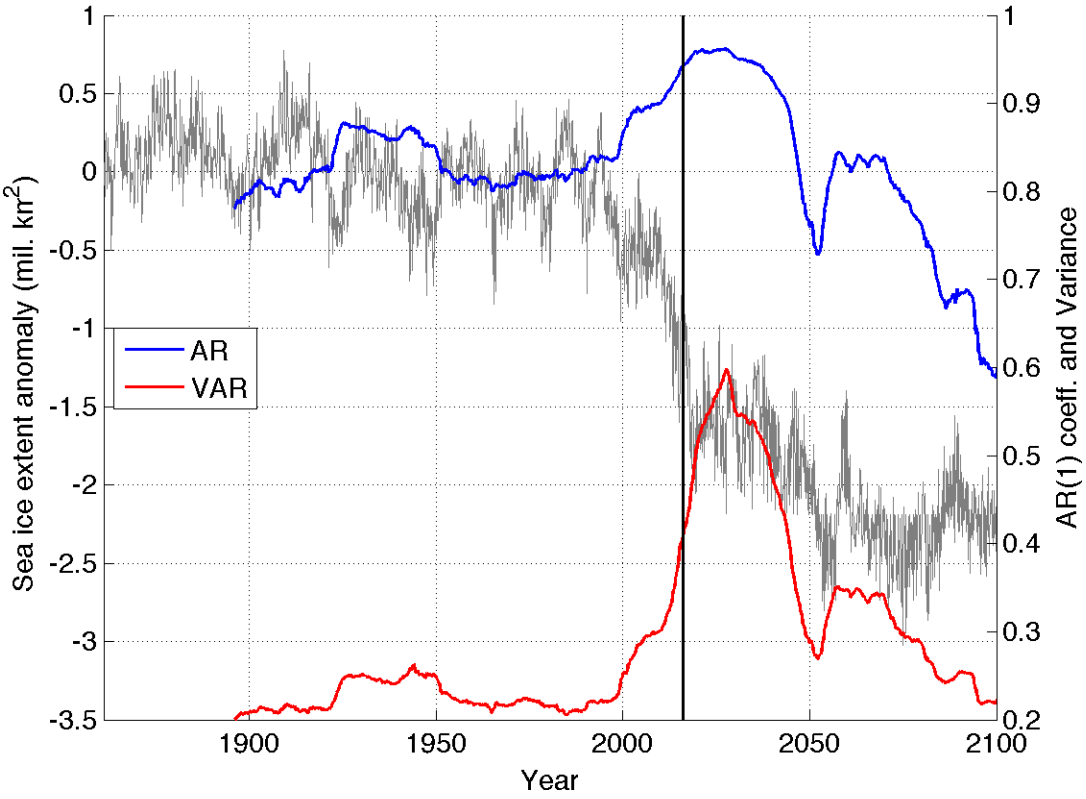

Figure 7. Sea ice extent anomalies (relative to 1901-1950 mean; $mil.km^2$) averaged over 40°N to 90°N for the MIROC-ESM-CHEM model from 1861 to 2100 (grey line). Autocorrelation coefficients (AR; blue line) and variance (VAR; red line), measured as the standard deviation, for a window size of 35 years. Thick, black vertical line denotes the transition year (2016).

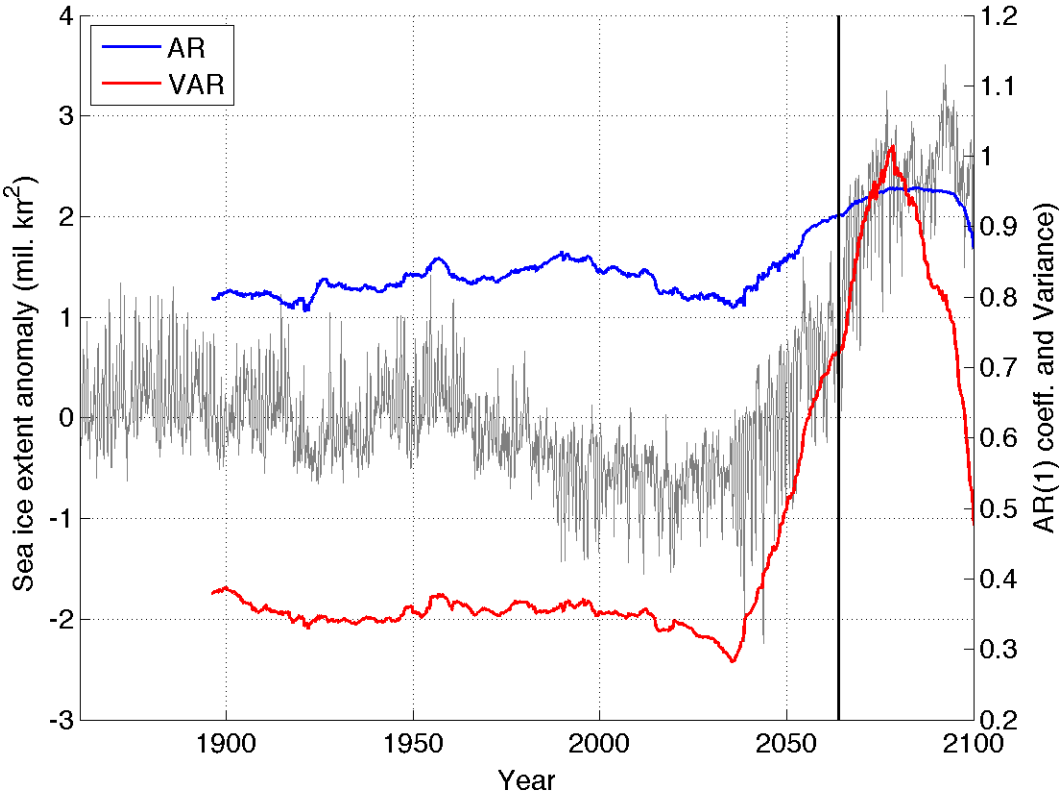

Figure 8. Sea ice extent anomalies (relative to 1901-1950 mean; $mil.km^2$) averaged over 40°N to 90°N for the FIO-ESM model from 1861 to 2100 (grey line). Autocorrelation coefficients (AR; blue line) and variance (VAR; red line), measured as the standard deviation, for a window size of 35 years. Thick, black vertical line denotes the transition year (2064).

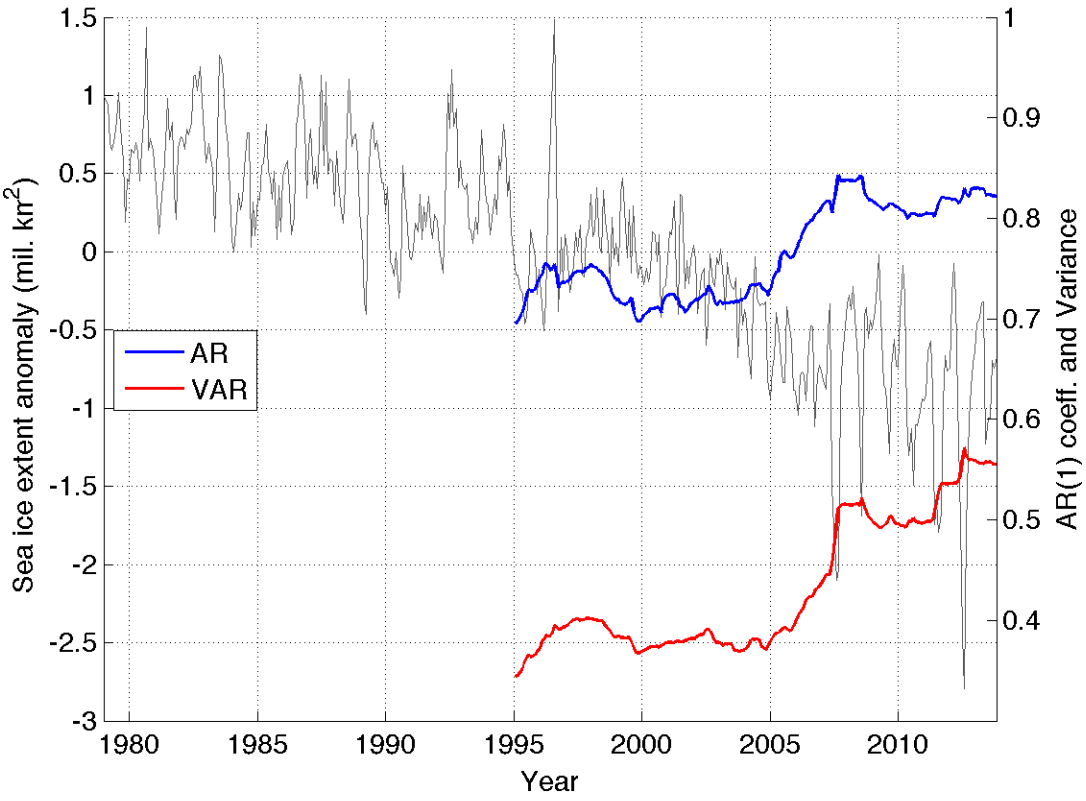

Figure 9. Observed sea ice extent anomalies (relative to 1951-1980 mean; $mil.\,km^2$) averaged over 40°N to 90°N for the period 1979-2013 (grey line). Autocorrelation coefficients (AR; blue line) and variance (VAR; red line), measured as the standard deviation, for a window size of 16 years.

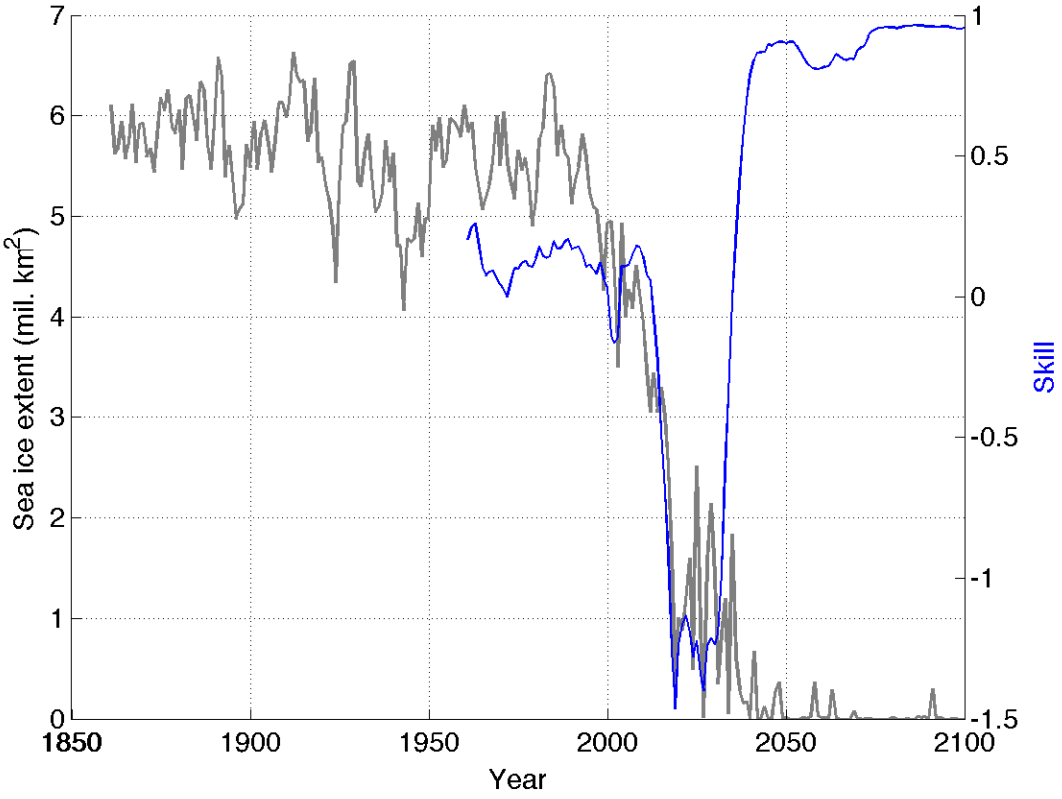

Figure 10a. MIROC-ESM-CHEM September sea ice extent ($mil.km^2$) averaged over 40°N to 90°N (grey line). Blue line is the forecast skill (relative to a CLIPER forecast) for the month of September, averaged over all analog forecast periods.

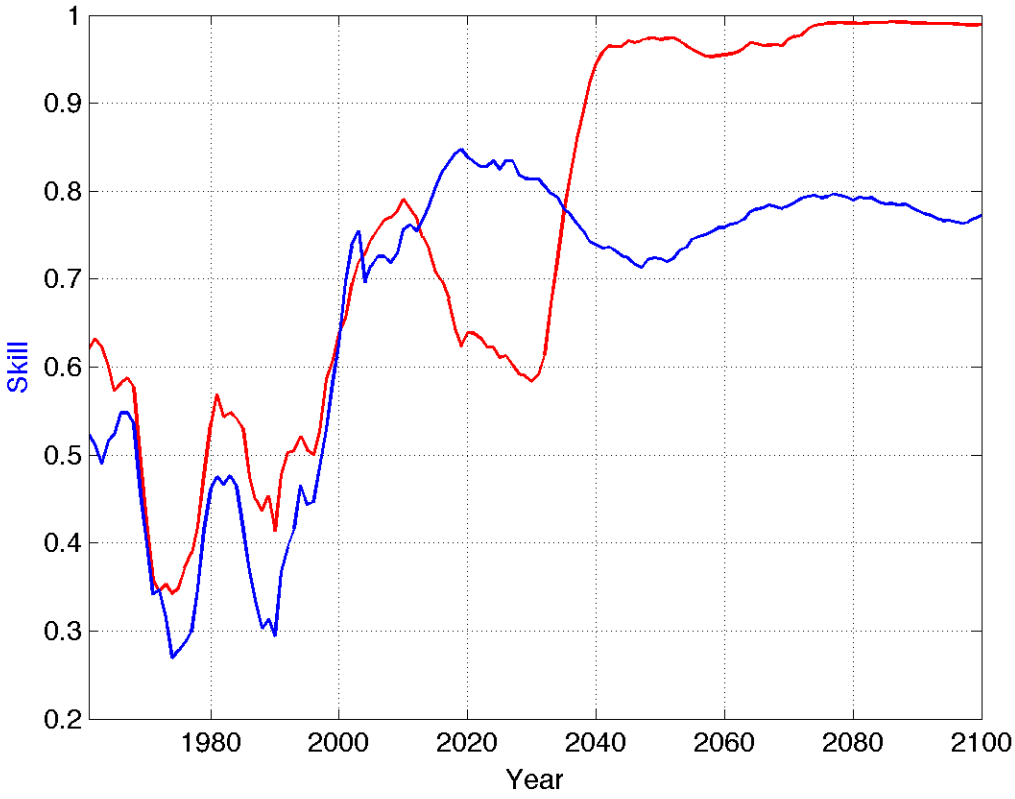

Figure 10b. Mean skill relative to climatology for an analog forecast (red) and CLIPER forecast (blue) for MIROC-ESM-CHEM September sea ice extent.

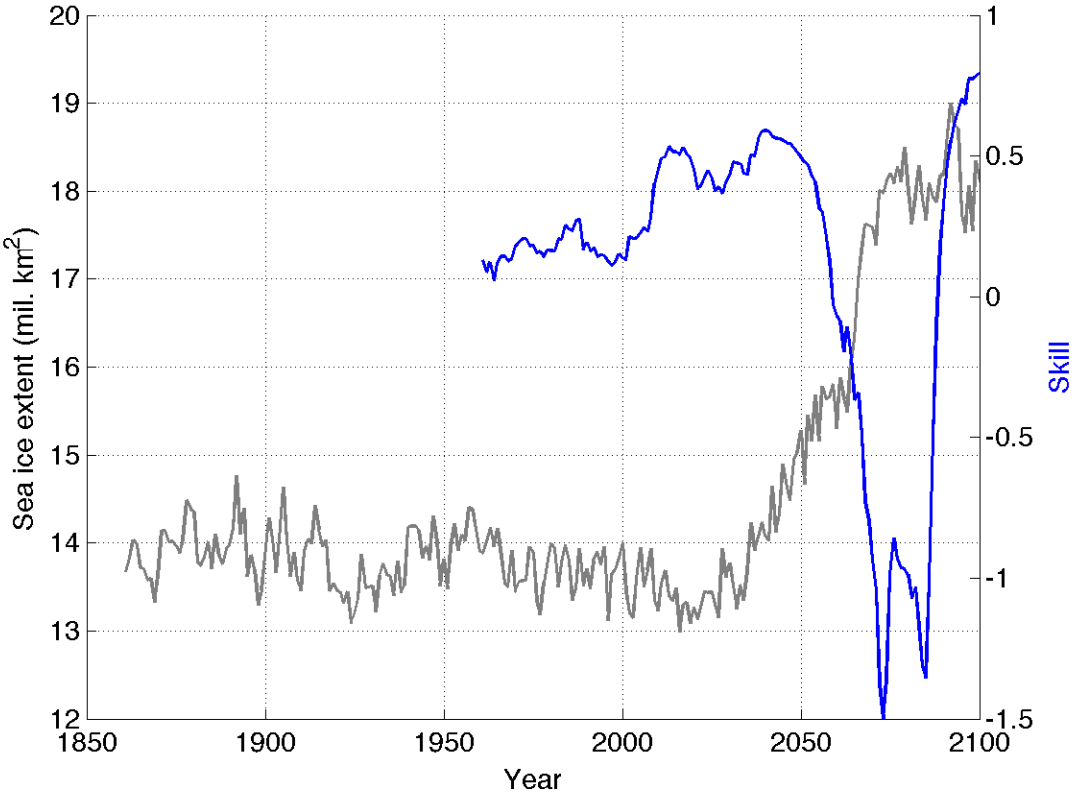

Figure 11a. FIO-ESM March sea ice extent ($mil.km^2$) averaged over 40°N to 90°N (grey line). Blue line is the forecast skill (relative to a CLIPER forecast) for the month of March, averaged over all analog forecast periods.

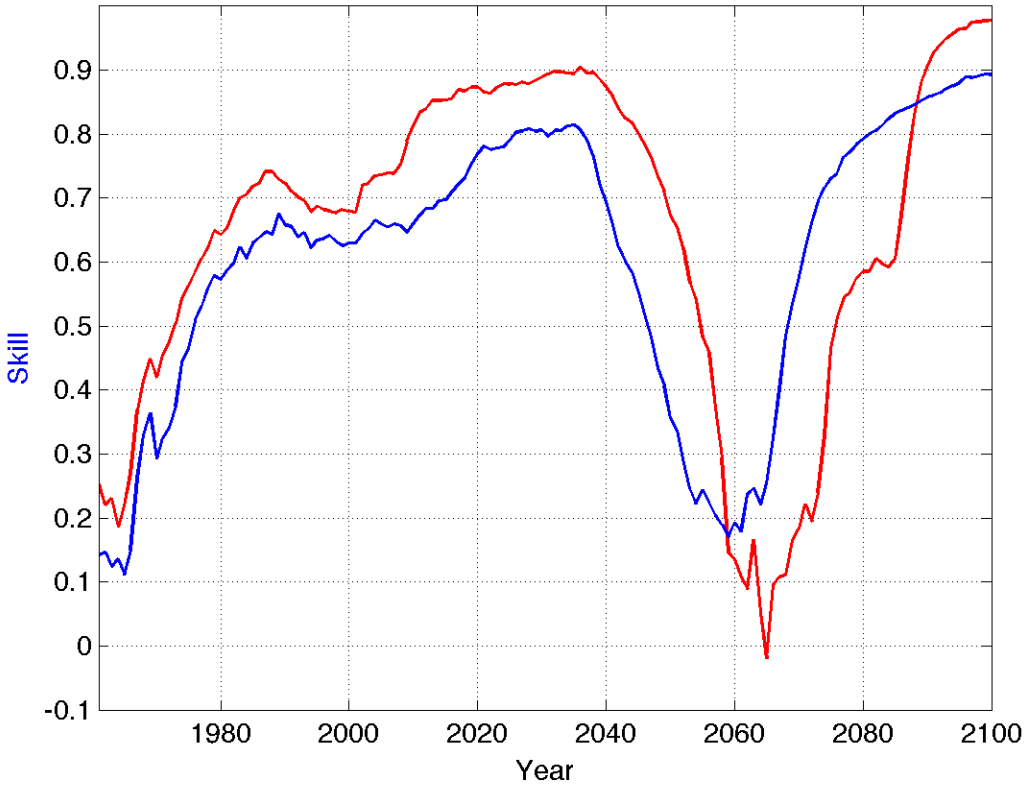

Figure 11b. Mean skill relative to climatology for an analog forecast (red) and CLIPER forecast (blue) for FIO-ESM March sea ice extent.

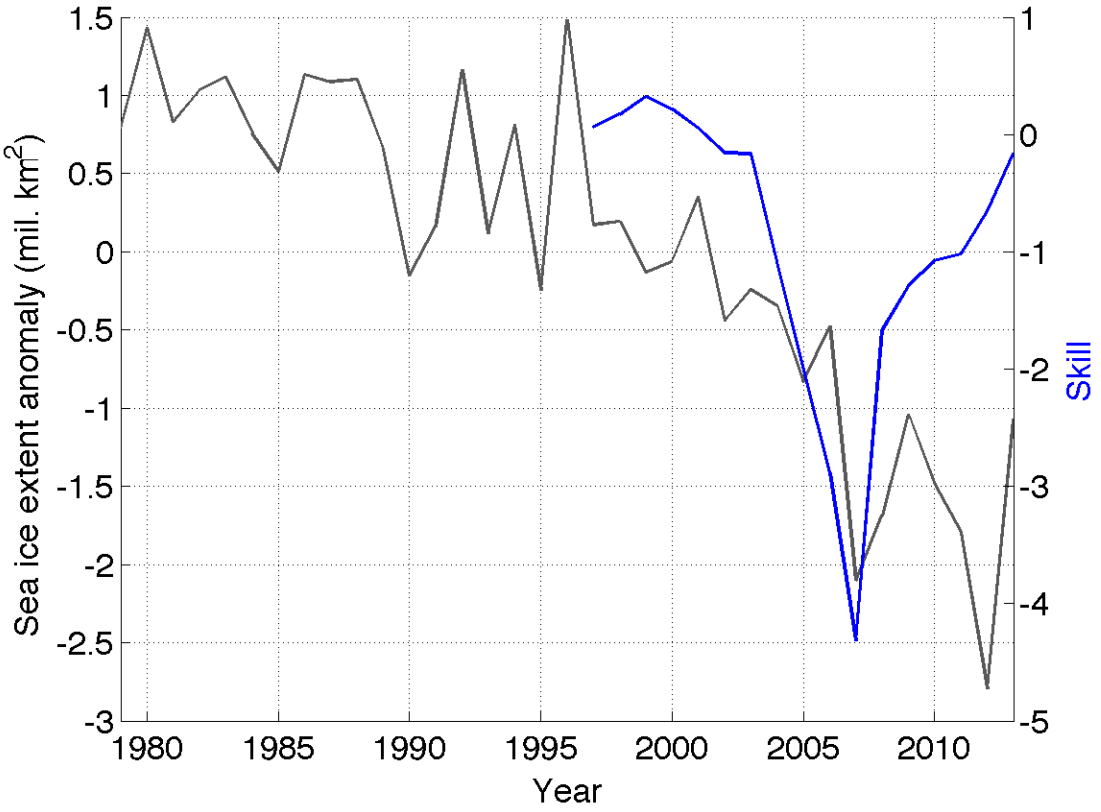

Figure 12. Observed September sea ice extent anomaly ($mil.km^2$) averaged over 40°N to 90°N (black line). Blue line is the mean skill (relative to a CLIPER forecast) for all analog forecast periods.

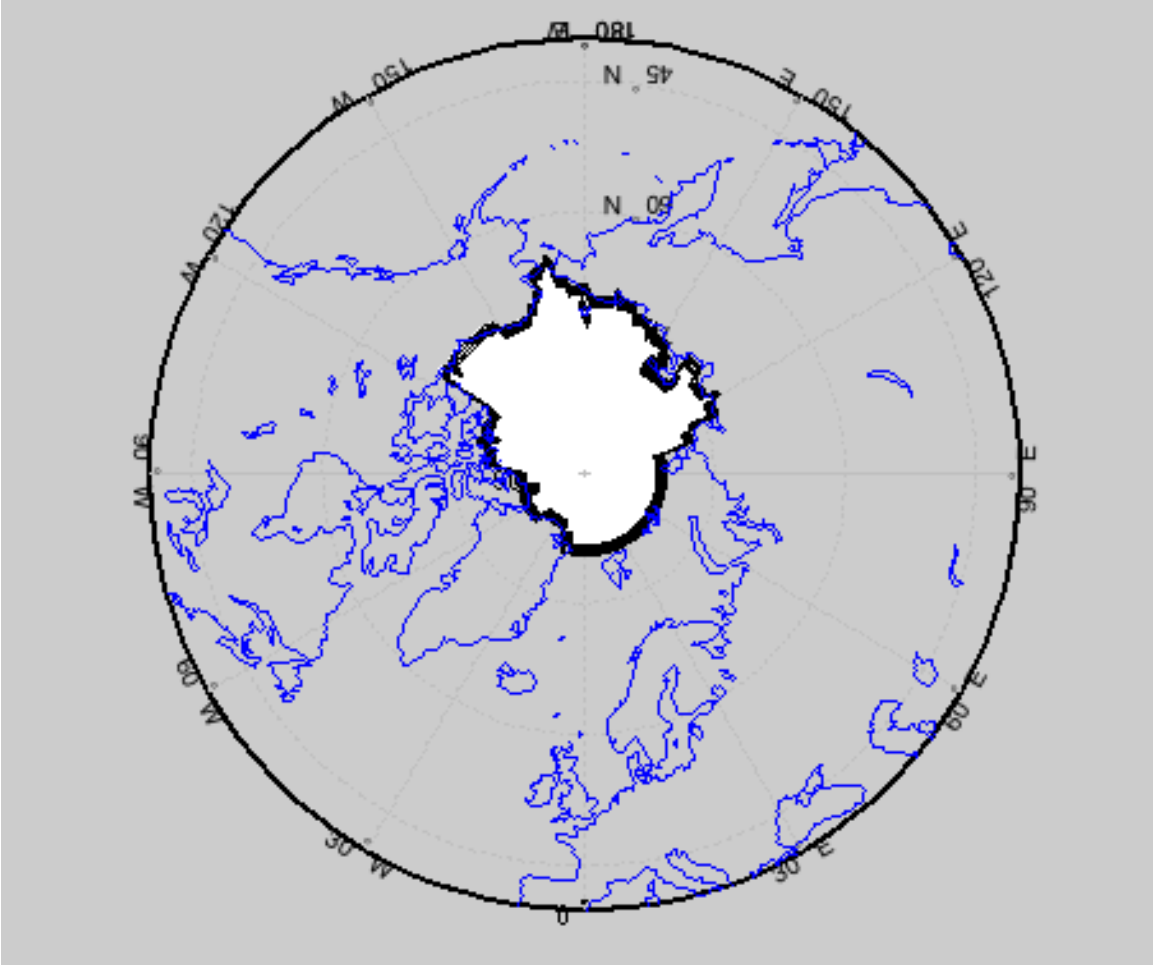

Figure 13a. Arctic Ocean sub-region used for the regional analysis of the MIROC-ESM-CHEM model.

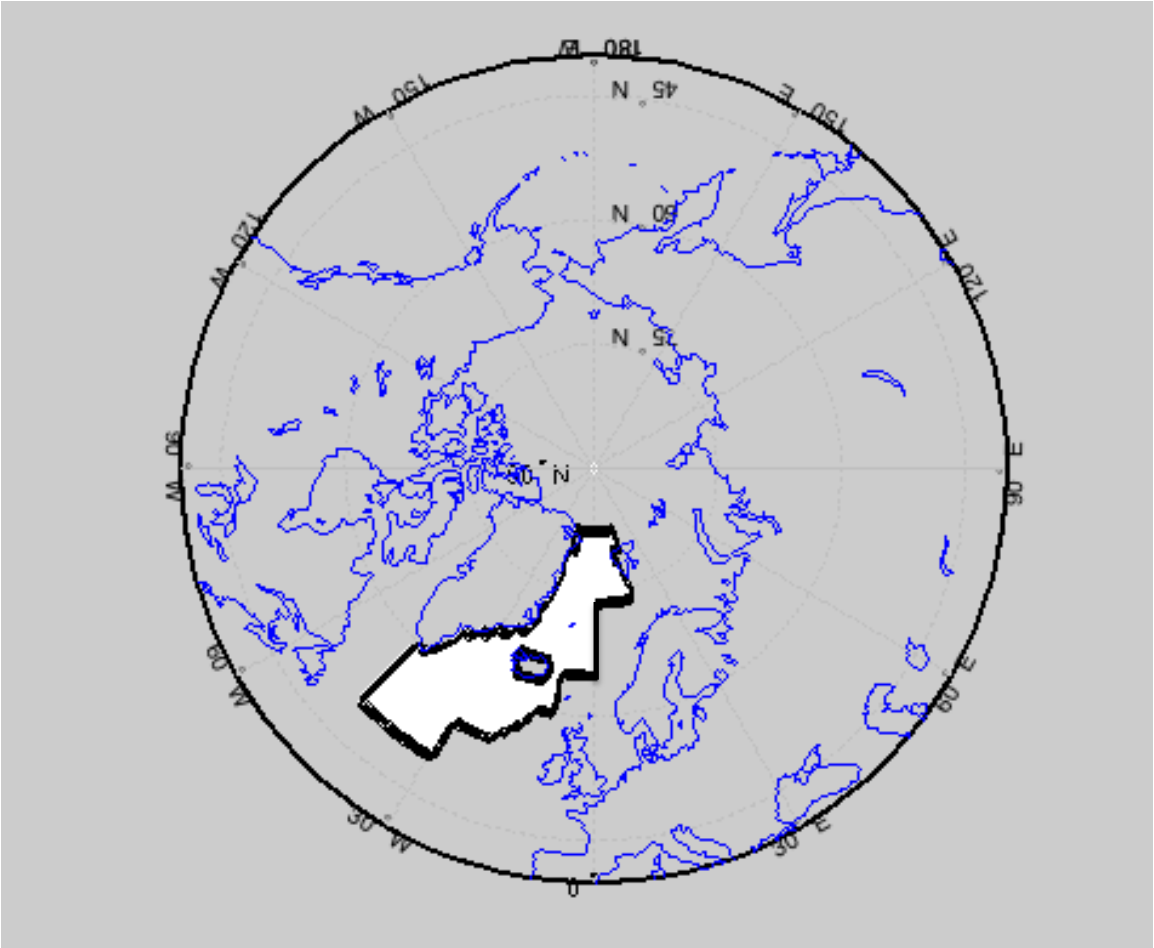

Figure 13b. Greenland Sea sub-region used for the regional analysis of the FIO-ESM model.

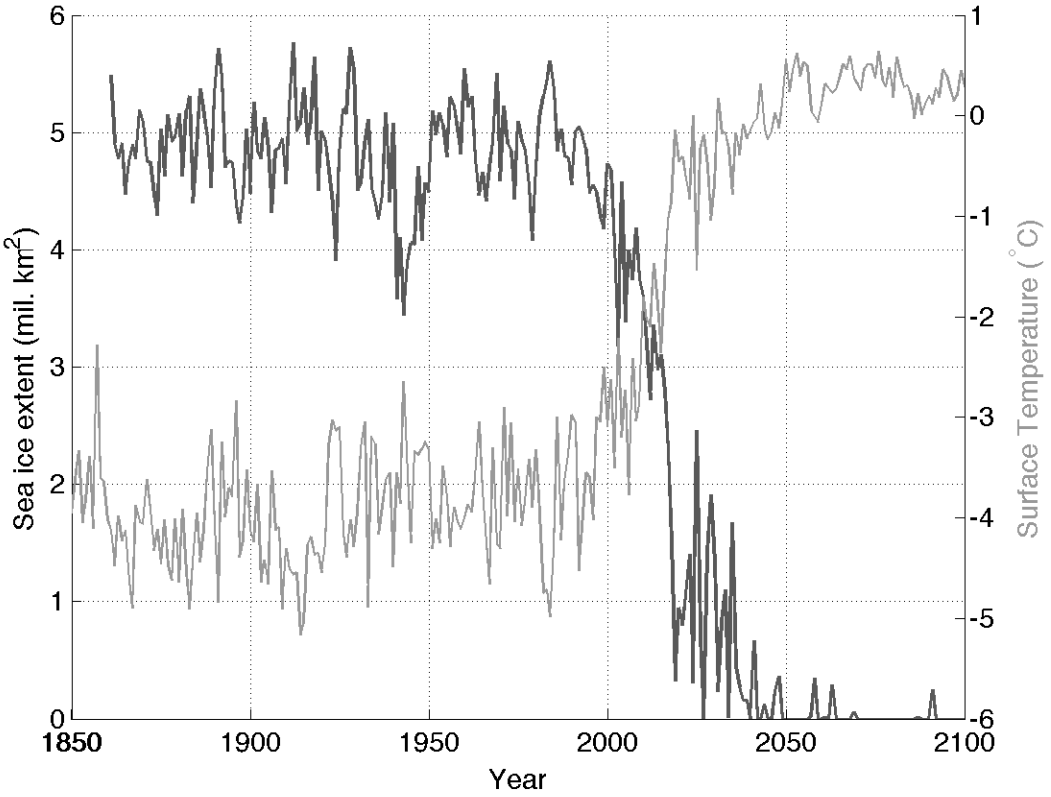

Figure 14. Sea ice extent ($mil.km^2$) and surface temperature (°C) averaged over the Arctic Ocean for the MIROC-ESM-CHEM model for September from 1861-2100 and 1850-2100, respectively.

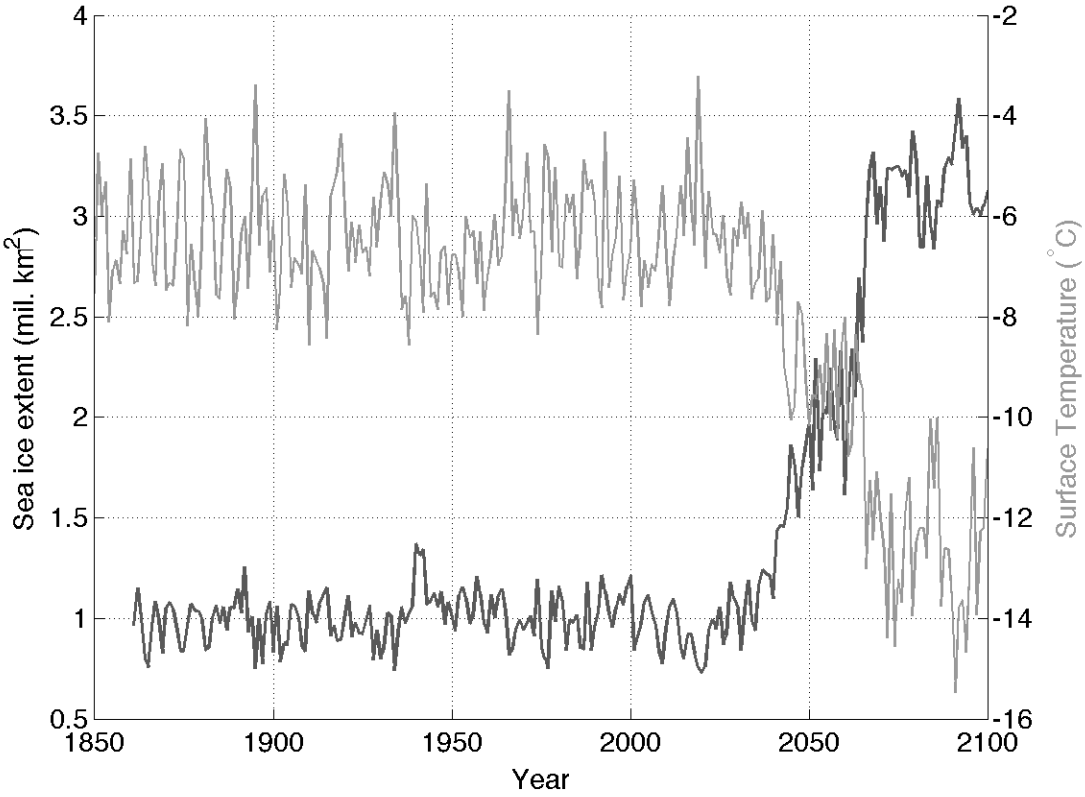

Figure 15. Sea ice extent ($mil.km^2$) and surface temperature (°C) averaged over the Greenland Sea for the FIO-ESM model for March from 1861-2100 and 1850-2100, respectively.

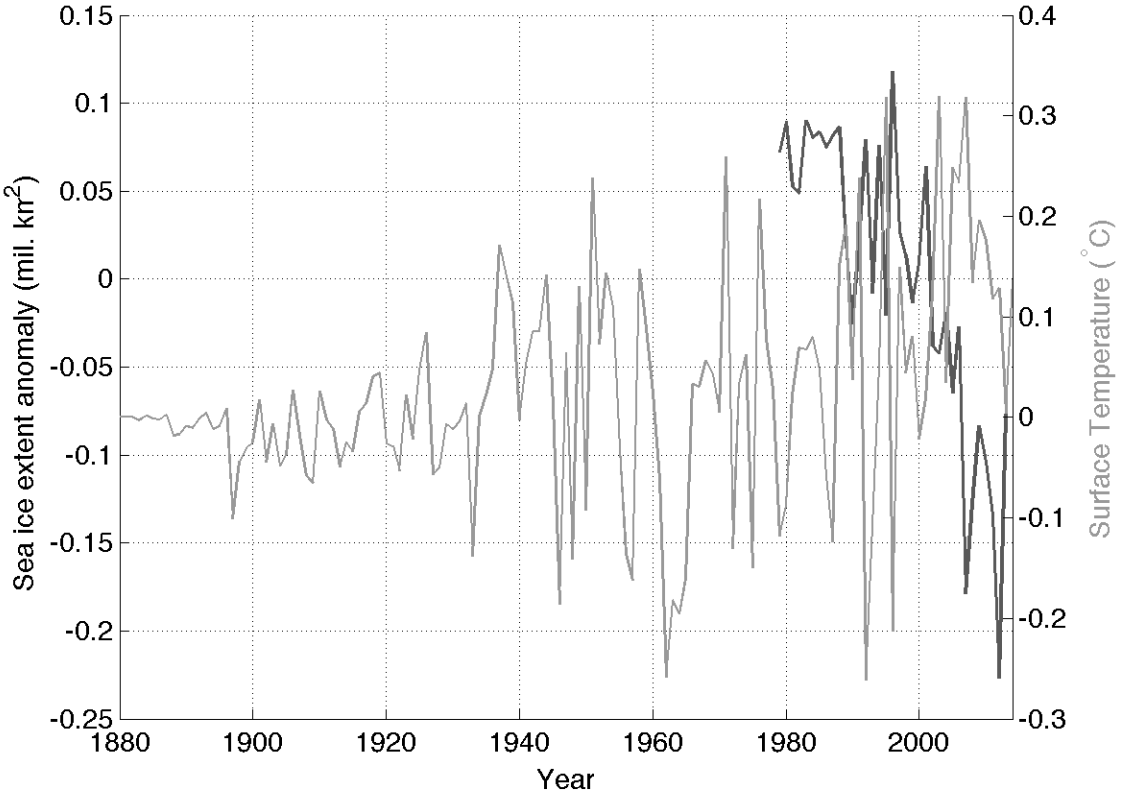

Figure 16. Observed sea ice extent anomaly and surface temperature anomaly (°C) averaged over the Arctic Ocean for September from 1979-2013 and 1880-2014 respectively.

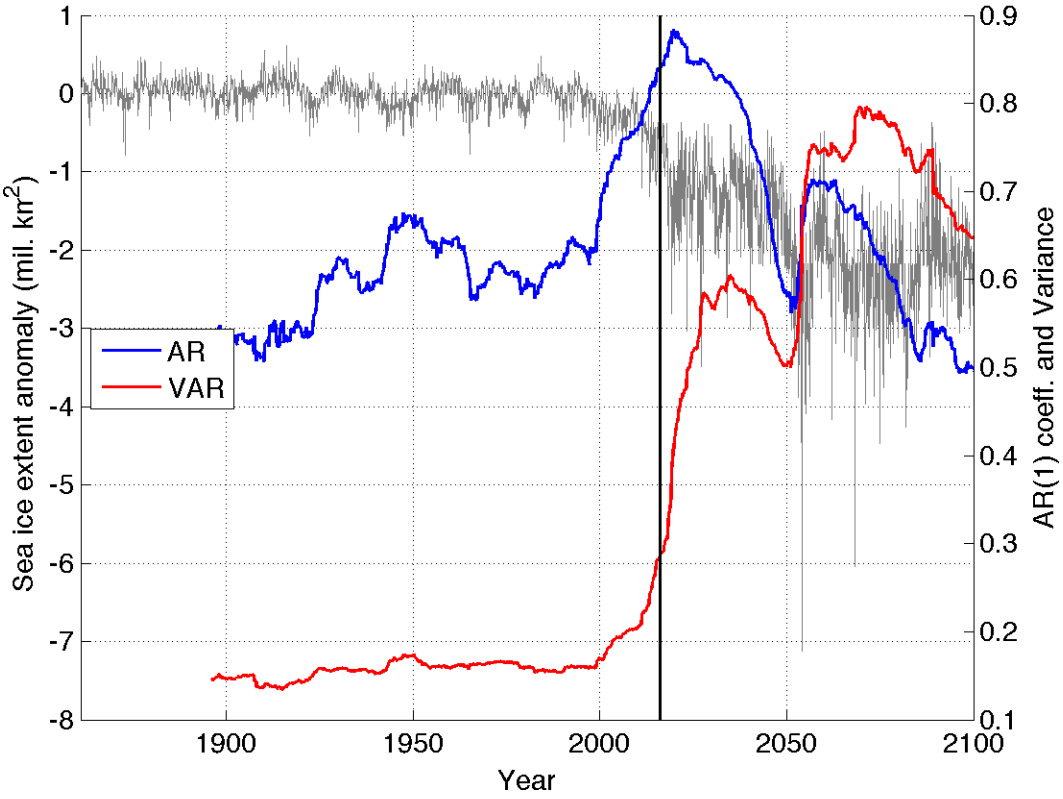

Figure 17. Sea ice extent anomalies (relative to 1901-1950 mean; $mil.km^2$) averaged over the Arctic Ocean for the MIROC-ESM-CHEM model from 1861 to 2100 (grey line). Autocorrelation coefficients (AR; blue line) and variance (VAR; red line), measured as the standard deviation, for a window size of 35 years. Thick, black vertical line denotes the transition year (2016).

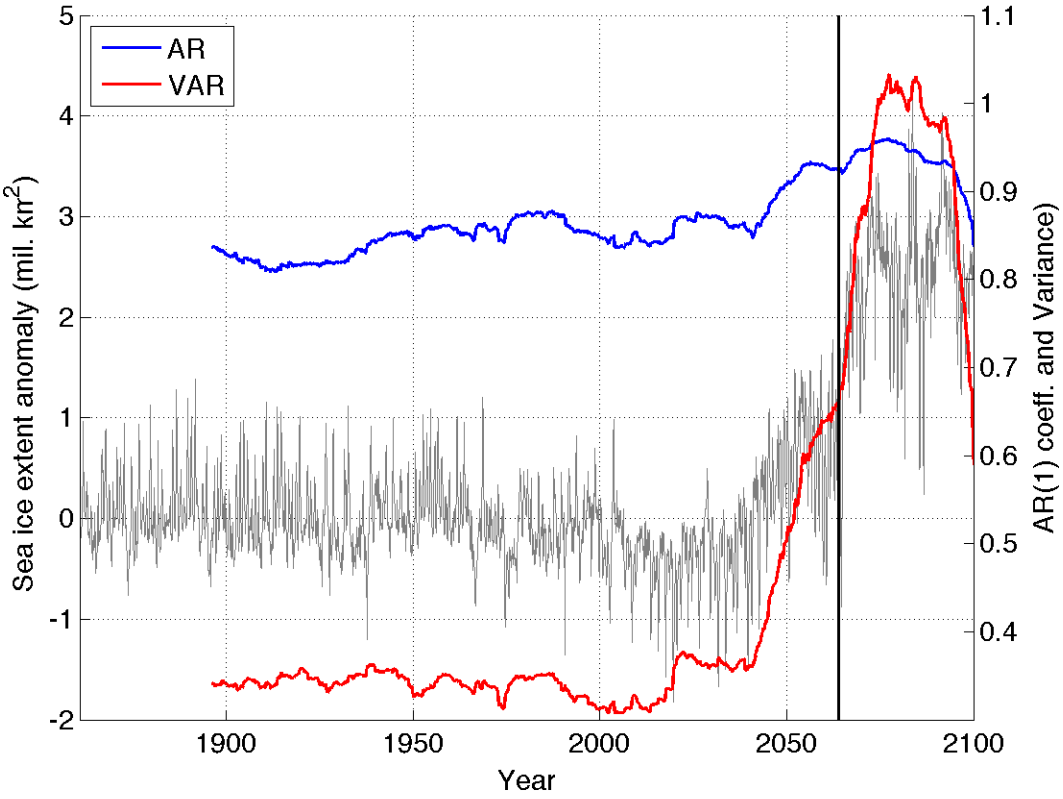

Figure 18. Sea ice extent anomalies (relative to 1901-1950 mean; $mil.km^2$) averaged over the Greenland Sea for the FIO-ESM model from 1861 to 2100 (grey line). Autocorrelation coefficients (AR; blue line) and variance (VAR; red line), measured as the standard deviation, for a window size of 35 years. Thick, black vertical line denotes the transition year (2064).

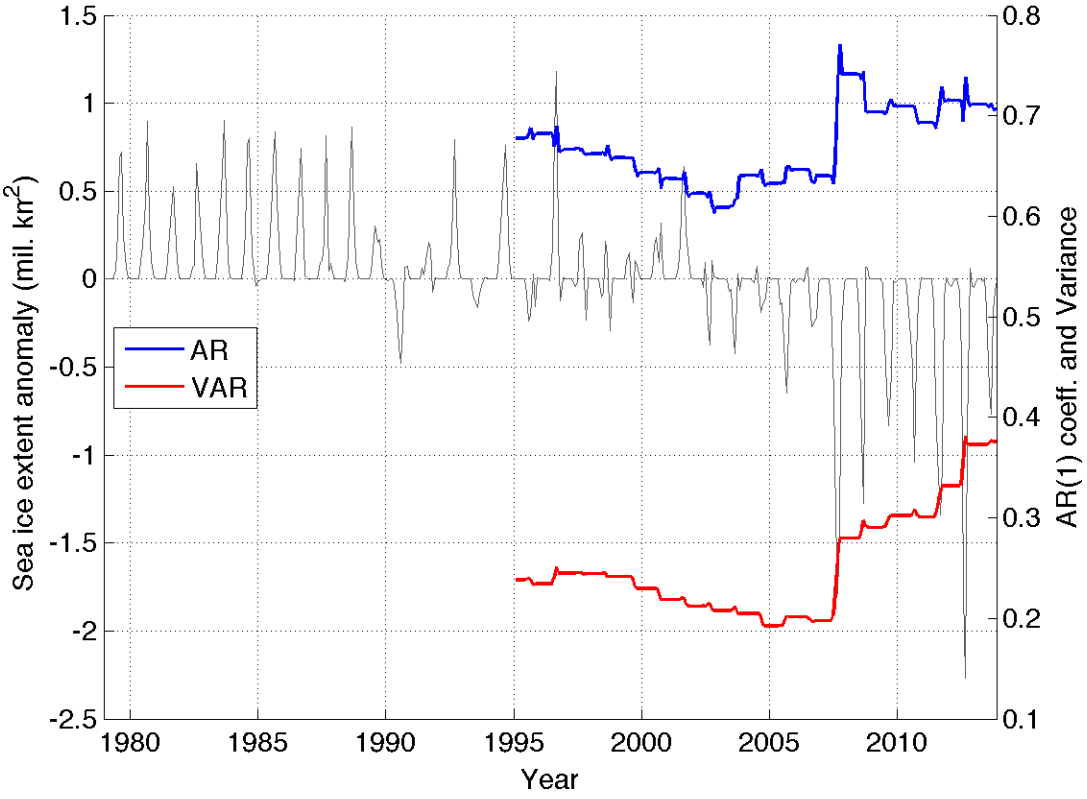

Figure 19. Observed sea ice extent anomalies (relative to 1951-1980 mean; $mil.\,km^2$) averaged over the Arctic Ocean for the period 1979-2013 (grey line). Autocorrelation coefficients (AR; blue line) and variance (VAR; red line), measured as the standard deviation, for a window size of 16 years.

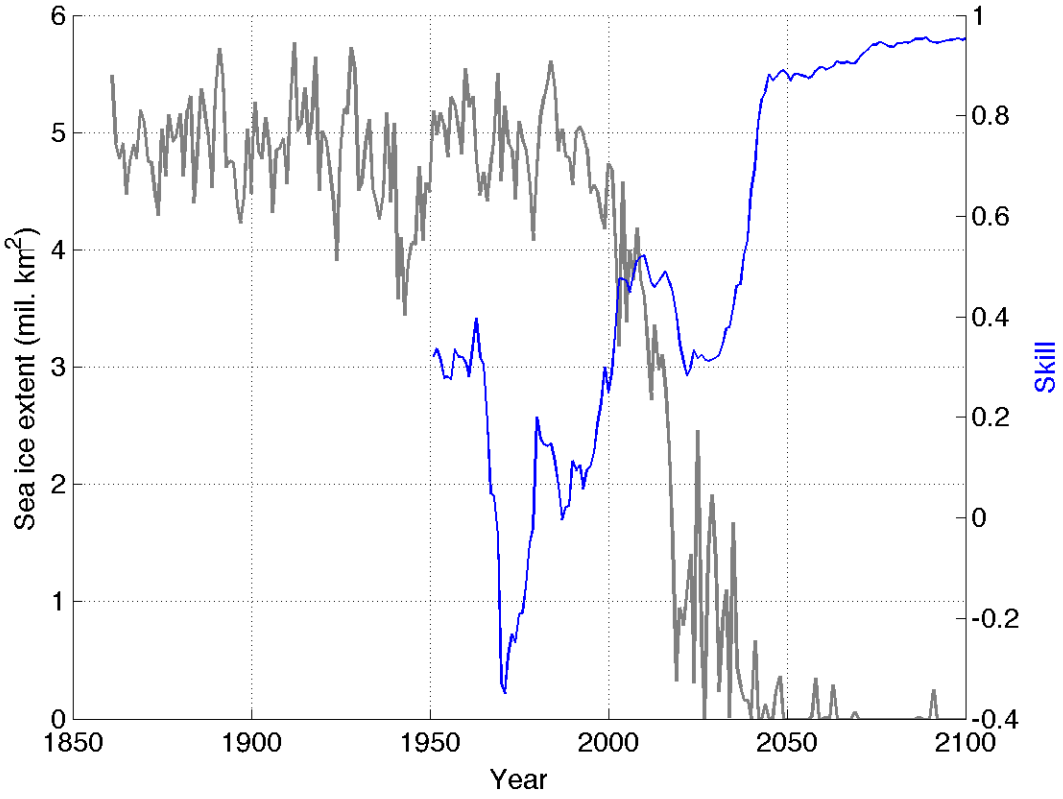

Figure 20a. MIROC-ESM-CHEM September sea ice extent ($mil.km^2$) averaged over the Arctic Ocean (grey line). Blue line is the forecast skill (relative to climatology) for the month of September, averaged over all analog forecast periods.

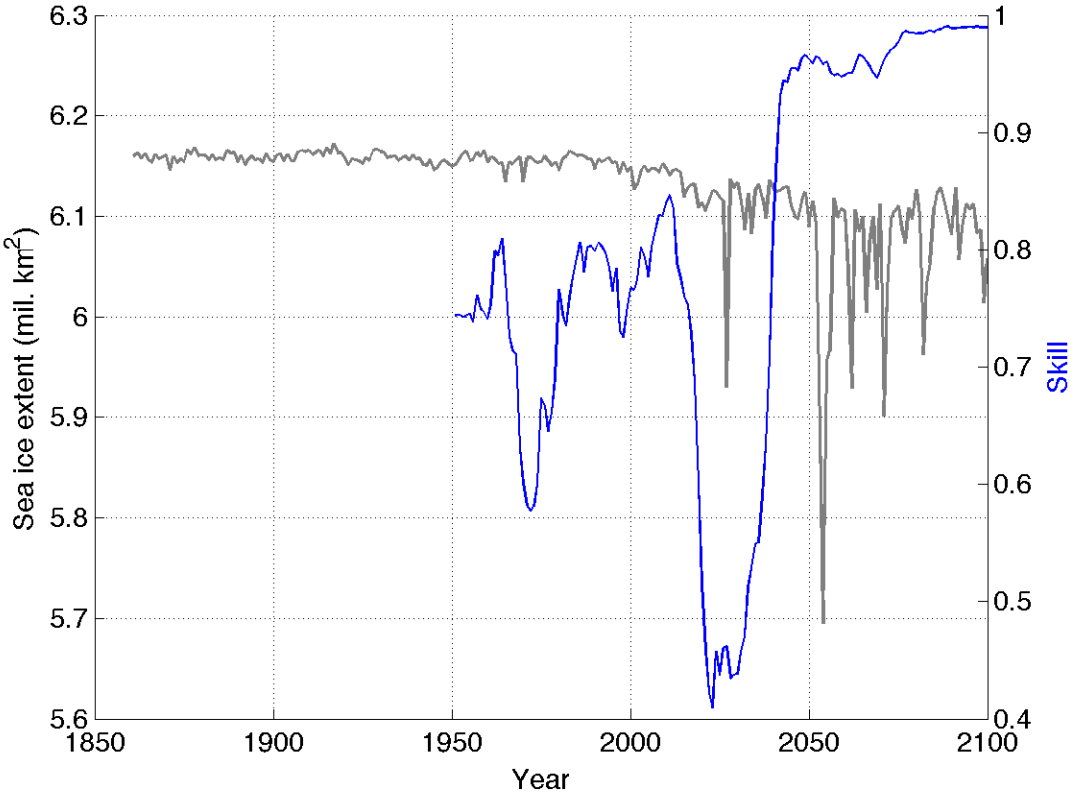

Figure 20b. MIROC-ESM-CHEM February sea ice extent ($mil.\,km^2$) averaged over the Arctic Ocean (grey line). Blue line is the forecast skill (relative to climatology) for the month of February, averaged over all analog forecast periods.

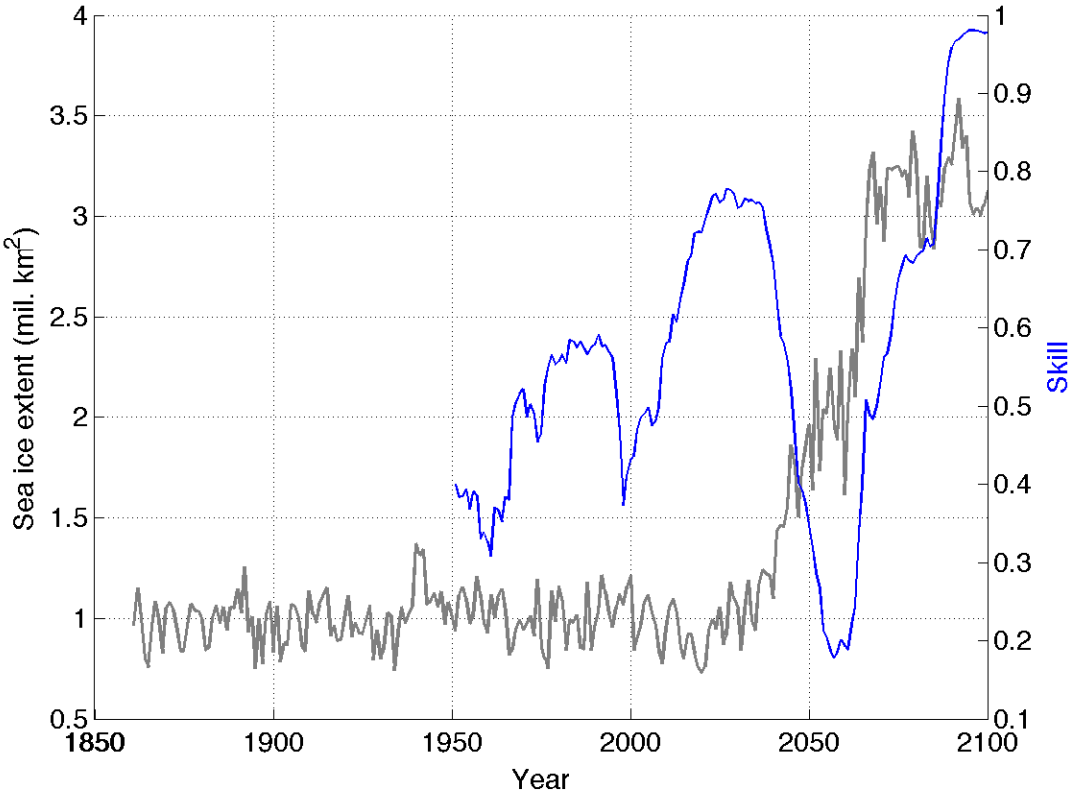

Figure 21. FIO-ESM March sea ice extent ($mil.km^2$) averaged over Greenland (grey line). Blue line is the forecast skill (relative to climatology) for the month of March, averaged over all analog forecast periods.

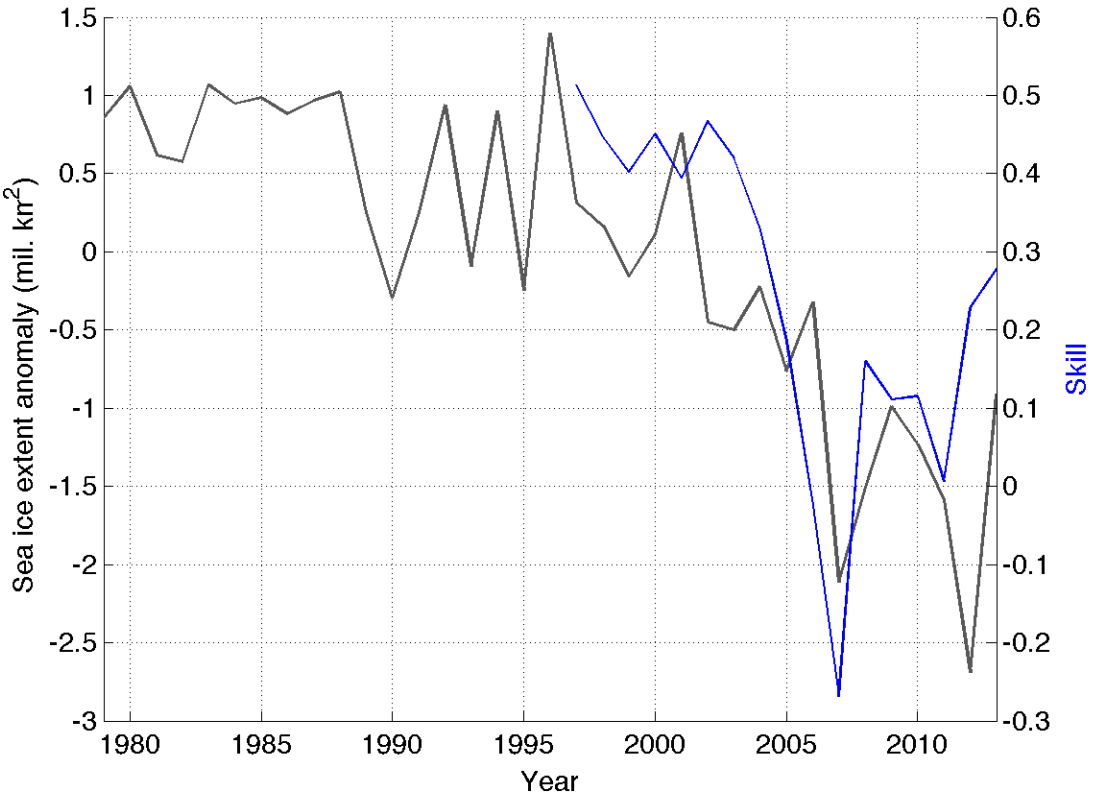

Figure 22. Observed September sea ice extent anomaly ($mil.km^2$) averaged over the Arctic Ocean (grey line). Blue line is the mean skill (relative to a CLIPER forecast) for all analog forecast periods.

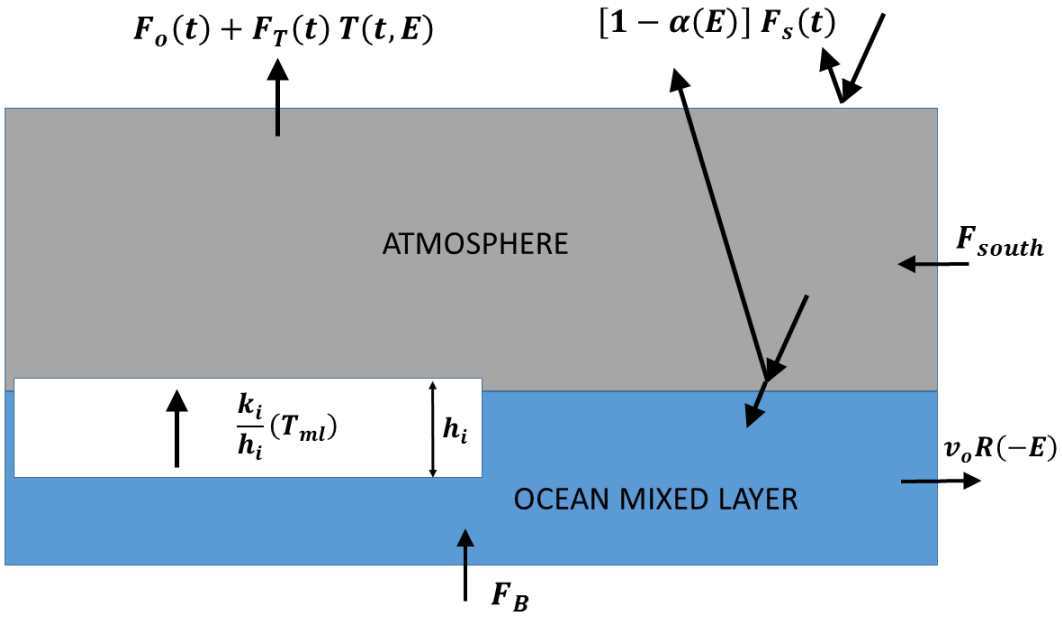

Figure 23. Schematic of the thermodynamic and dynamic $[v_0\ R(-E)]$ components of the stochastic sea ice model used in this study, which is a single column representation of the atmosphere, sea ice and ocean mixed layer.

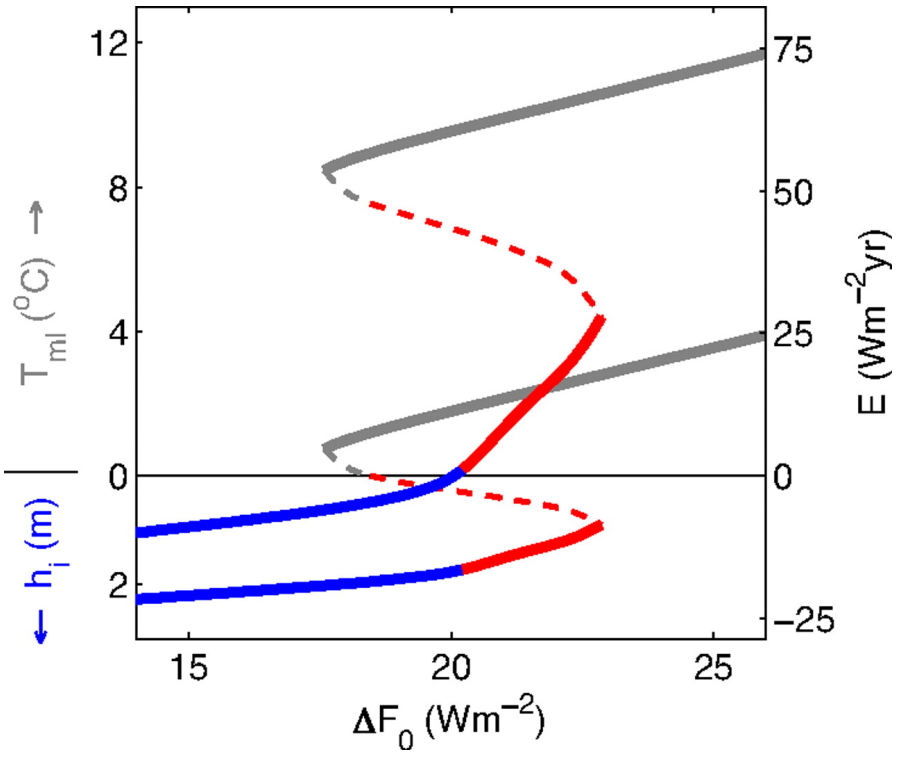

Figure 24. Diagram showing the bifurcation behavior within the stochastic sea ice model (Figure 3 from EW09). For each value of the imposed surface flux ΔF_o, the model is run until is converges on a steady-state seasonal cycle. The annual maximum and minimum values of E $(W\ m^{-2}\ yr)$ are plotted (right axis). The corresponding sea ice thickness in meters (h_i) or ocean mixed layer temperature in ℃ (T_{ml}) are plotted on the left axis. Perennial sea-ice conditions are indicated by the blue lines, the solid red lines indicate seasonally ice-free solutions, dashed red lines indicate unstable solutions and perennially ice-free conditions are marked by the grey lines.

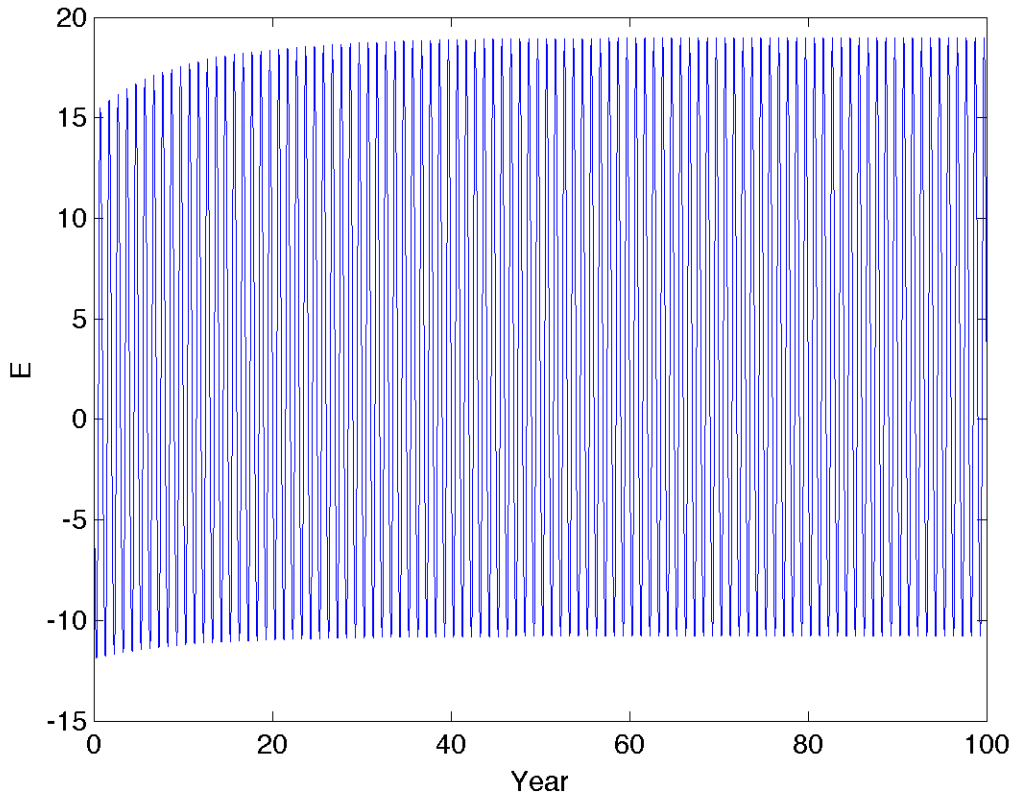

Figure 25a. Sample solution produced by the stochastic sea ice model with the following parameters: $\Delta F_o = 22.25\ Wm^{-2}, E(1,1) = 0\ Wm^{-2}\ yr$ and $S = 0\ Wm^{-2}$.

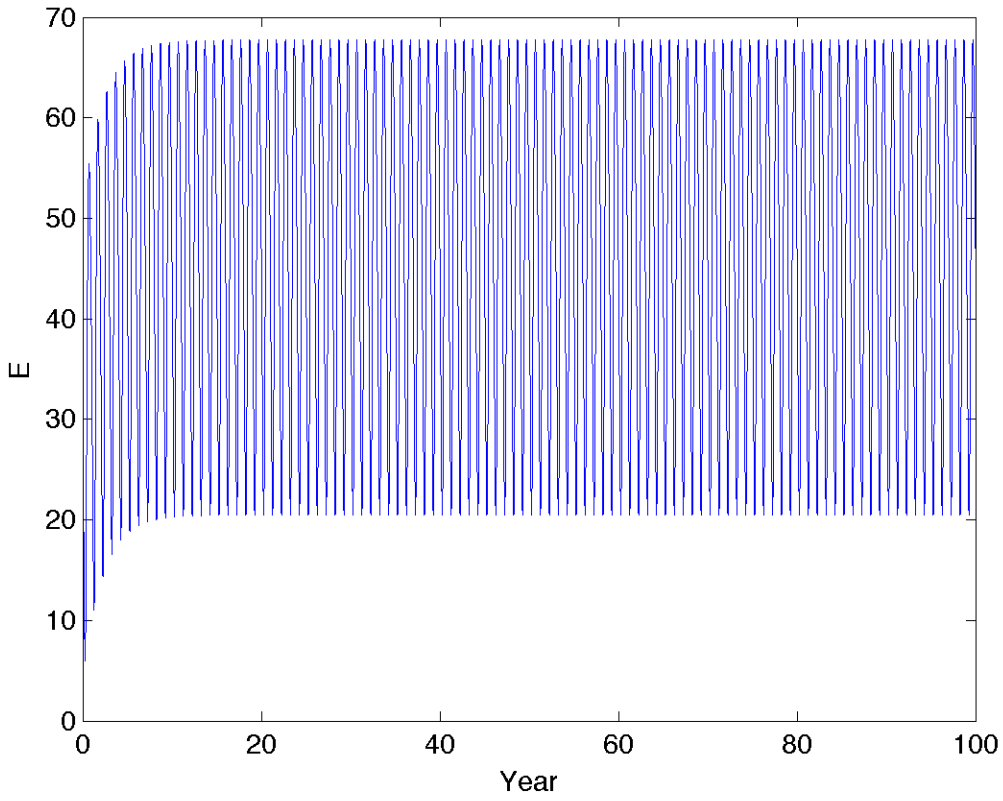

Figure 25b. Sample solution produced by the stochastic sea ice model with the following parameters: $\Delta F_o = 22.25\ Wm^{-2}, E(1,1) = 30\ Wm^{-2}\ yr$ and $S = 0\ Wm^{-2}$.

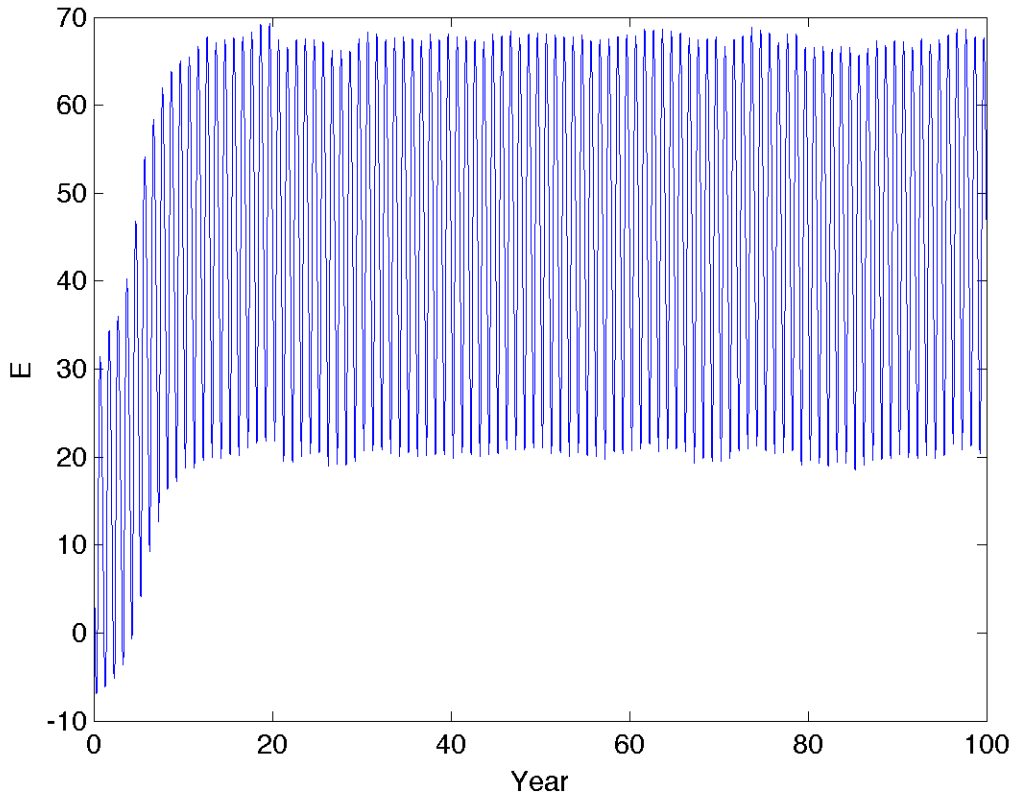

Figure 25c. Sample solution produced by the stochastic sea ice model with the following parameters: $\Delta F_o = 22.25\ Wm^{-2}, E(1,1) = 13\ Wm^{-2}\ yr$ and $S = 1\ Wm^{-2}$.

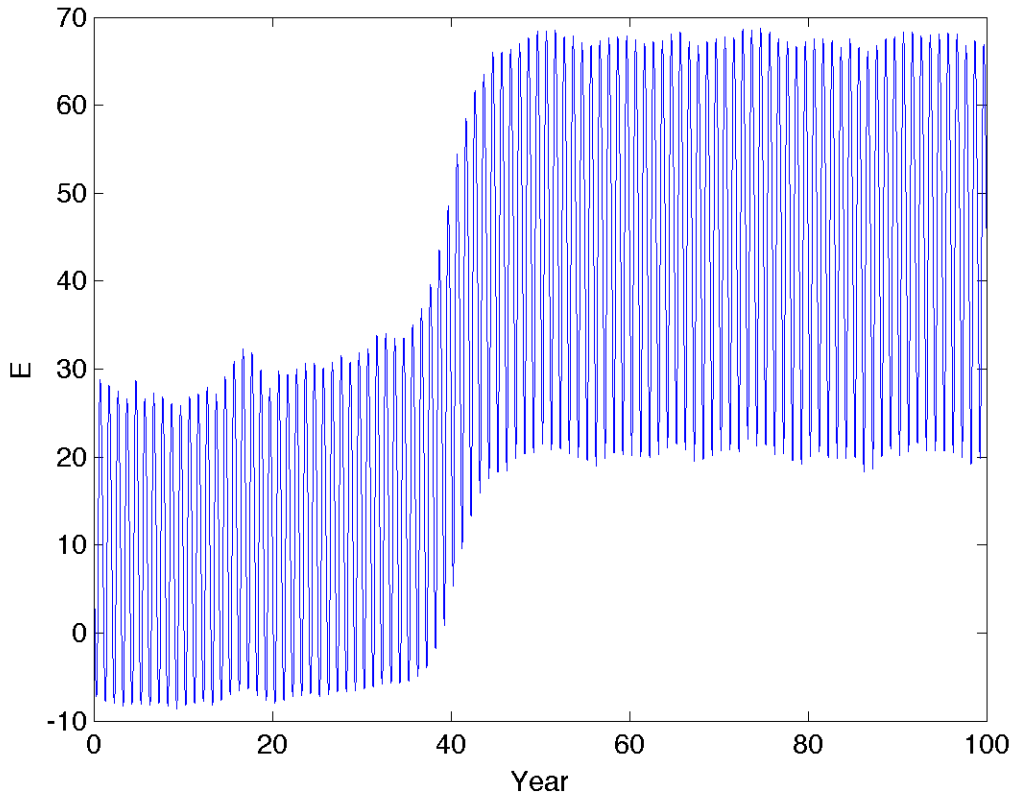

Figure 25d. Sample solution produced by the stochastic sea ice model with the following parameters: $\Delta F_o = 22.25\ Wm^{-2}, E(1,1) = 13\ Wm^{-2}\ yr$ and $S = 1\ Wm^{-2}$.

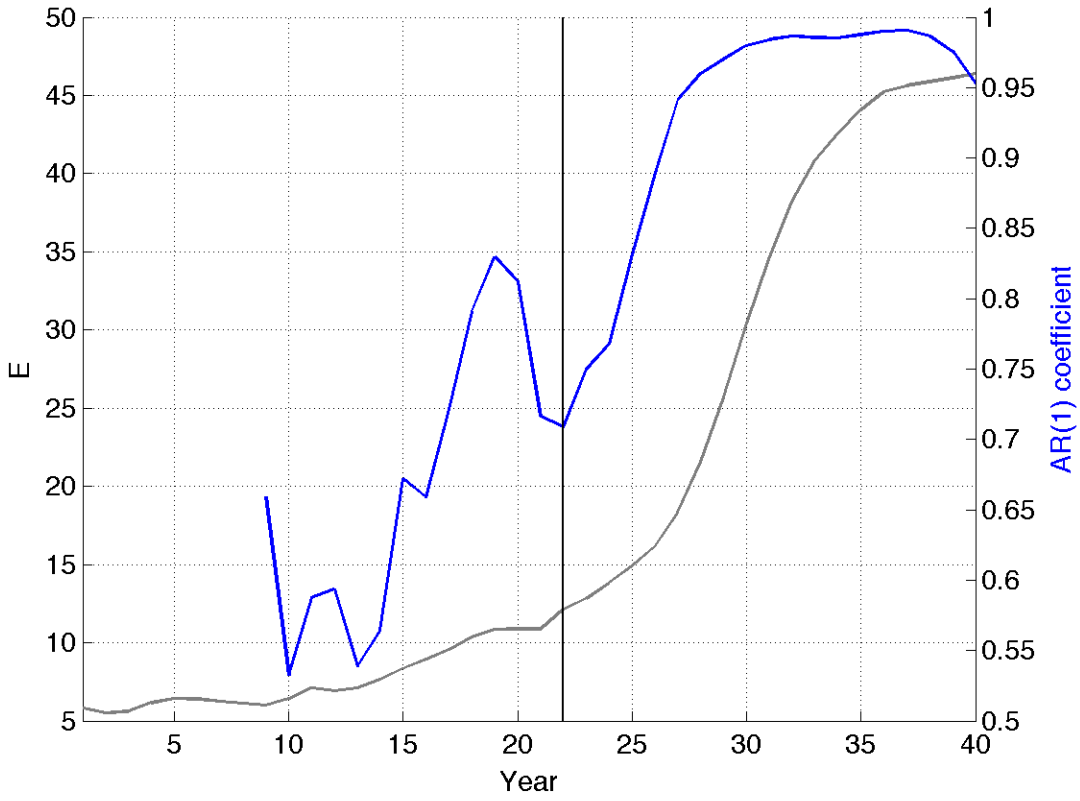

Figure 26a. Average of ten realizations of the stochastic sea ice model run with the following parameters: $\Delta F_o = 22.25\ Wm^{-2}, E(1,1) = 0\ Wm^{-2}\ yr\ and\ S = 1.05\ Wm^{-2}$ (grey line). Autocorrelation coefficients (blue line) for a window size of 7 years. Thick, black vertical line denotes the transition year (22).

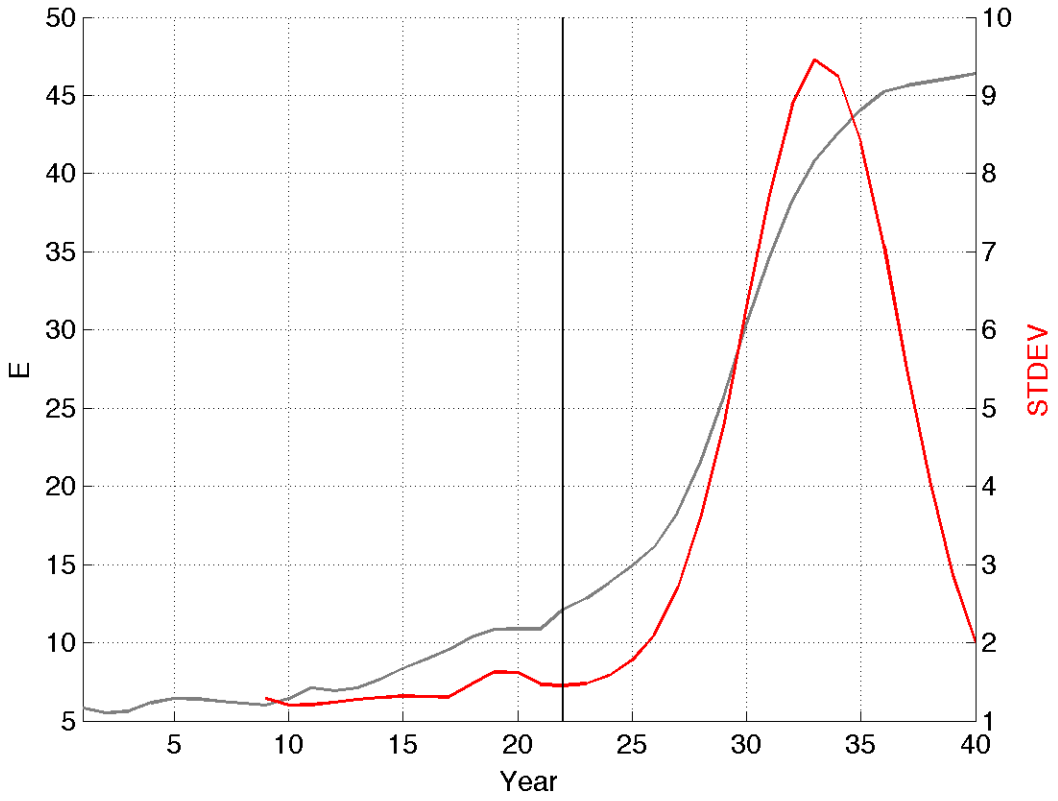

Figure 26b. Average of ten realizations of the stochastic sea ice model run with the following parameters: $\Delta F_o = 22.25\ Wm^{-2}, E(1,1) = 0\ Wm^{-2}\ yr\ and\ S = 1.05\ Wm^{-2}$ (grey line). Variance (blue line), measured as the standard deviation, for a window size of 7 years. Thick, black vertical line denotes the transition year (22).

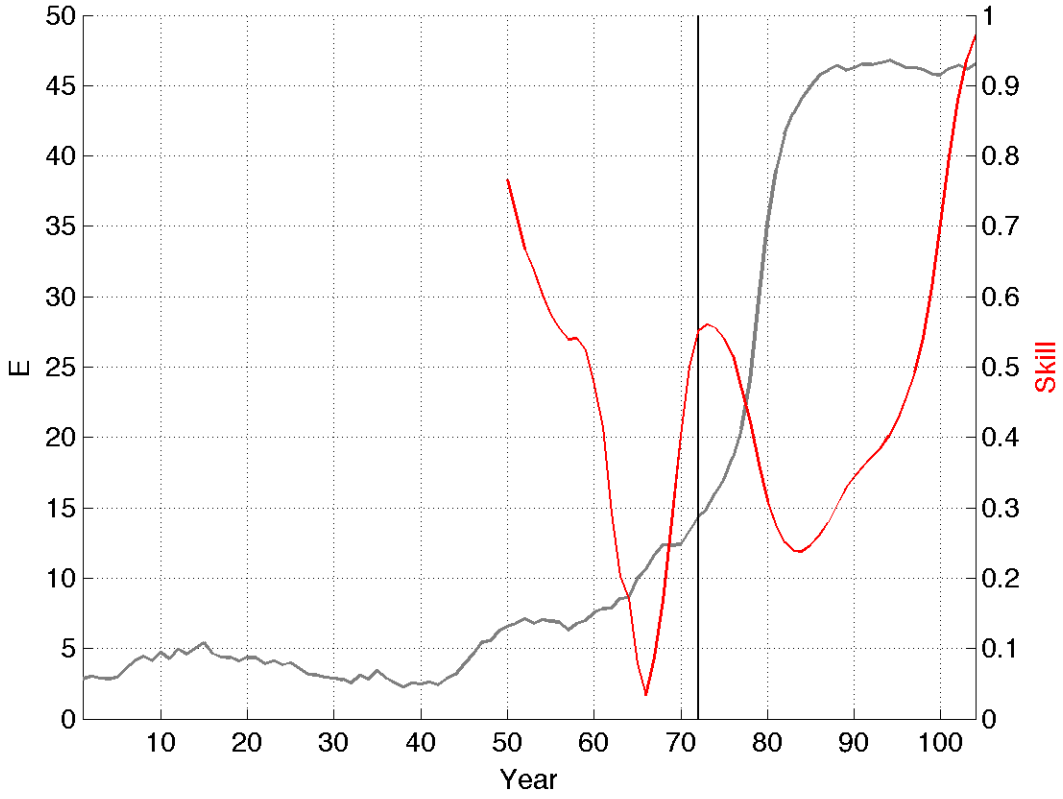

Figure 27. Average of ten realizations of the stochastic sea ice model run with the following parameters: $\Delta F_o = 22.25\ Wm^{-2}, E(1,1) = 0\ Wm^{-2}\ yr\ and\ S = 1.05\ Wm^{-2}$ (grey line). Red line is the forecast skill (relative to climatology), averaged over all analog forecast periods.

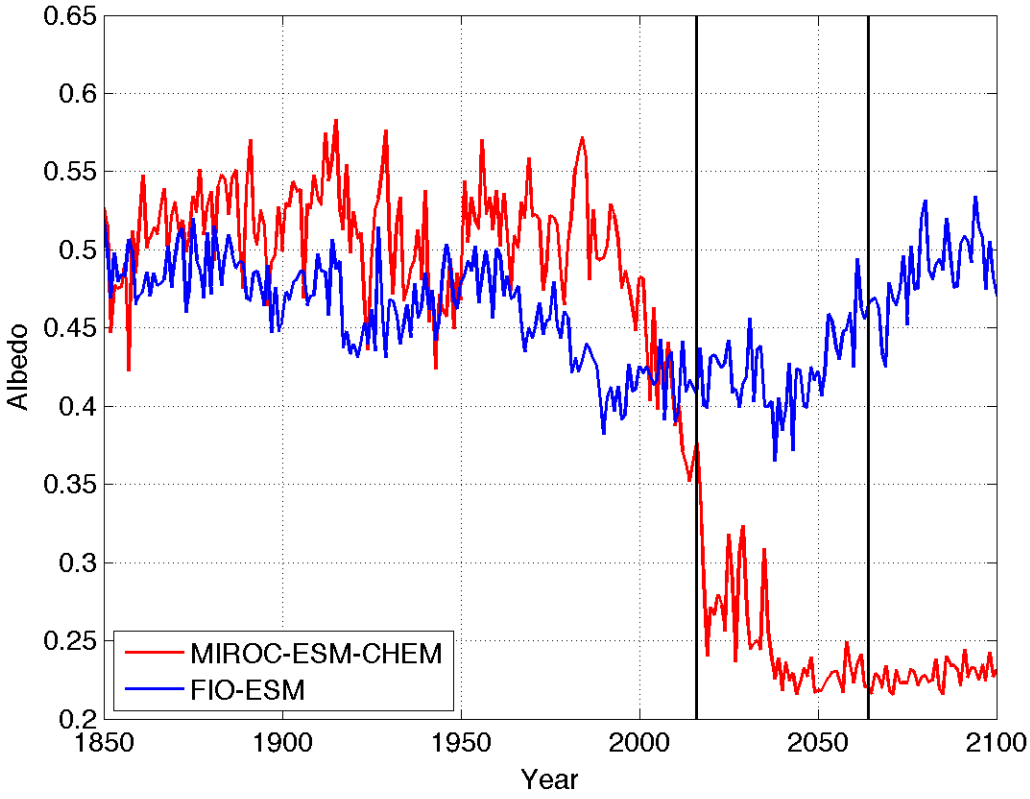

Figure 28a. Arctic surface albedo, estimated using the ratio of reflected shortwave radiation in the upward (rsus) and downward (rsds) directions, respectively. Thick, black vertical lines denote the year of sea ice transition in the MIROC-ESM-CHEM and FIO-ESM models respectively.

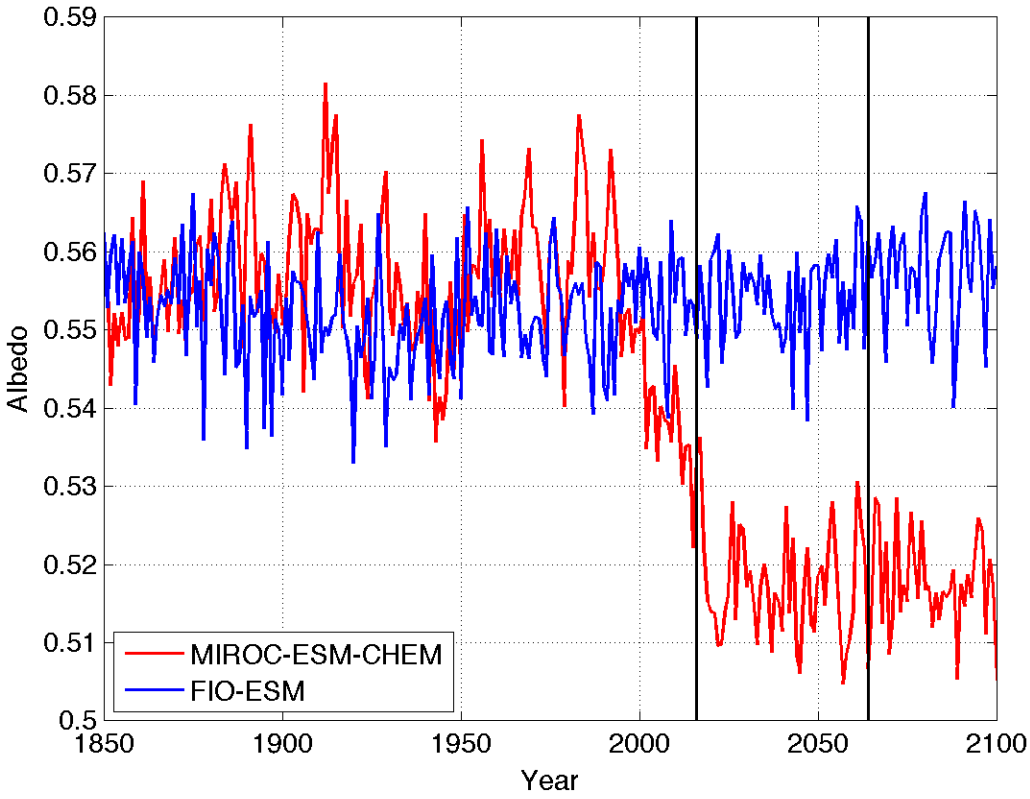

Figure 28b. As in Figure 28a; modeled Arctic albedo (top of atmosphere).

Symbol	Description	Value
L_i	Latent heat of fusion of ice	9.5 W m^{-3} yr
$c_{ml}H_{ml}$	Ocean mixed layer heat capacity times depth	6.3 W m^{-2} yr K^{-1}
α_i	Albedo for ice-covered ocean	0.68
α_{ml}	Albedo for ice-free ocean	0.2
k_i	Ice thermal conductivity	2 W m^{-1} K^{-1}
F_B	Heat flux into bottom of sea ice or mixed layer	2 W m^{-2}
h_α	Ice thickness range for smooth transition from α_i to α_{ml}	0.5 m
v_0	Dynamic export of ice	0.1 yr^{-1}
$F_0(t)$	Temperature-independent surface flux (varies by season- see below)	85 W m^{-2}
$F_T(t)$	Temperature-independent surface flux (varies by season- see below)	2.8 W m^{-1} K^{-1}
$F_s(t)$	Incident shortwave radiation flux (varies by season- see below)	100 W m^{-2}
ΔF_0	Imposed surface heat flux	0 W m^{-2}

Table 1. Definitions and magnitudes of stochastic sea ice model parameters. For the three seasonally varying parameters $F_0(t)$, $F_T(t)$ and $F_s(t)$, the table value is the annual average; the monthly means for January through December are:
$F_0(t) = [120\ 120\ 130\ 94\ 64\ 61\ 57\ 54\ 56\ 64\ 82\ 110]$ W m^{-2}, $F_T(t) = [3.1\ 3.2\ 3.3\ 2.9\ 2.6\ 2.6\ 2.5\ 2.5\ 2.6\ 2.7\ 3.1]$ W m^{-2} K^{-1} and
$F_s(t) = [0\ 0\ 30\ 160\ 280\ 310\ 220\ 140\ 59\ 6.4\ 0\ 0]$ W m^{-2}.

References

Abbot D, Silber M, Pierrehumbert R (2011) Bifurcations leading to summer Arctic sea ice loss. Journal of Geophysical Research 116: D19120. doi: 10.1029/2011JD015653.

Barnes L, Gruntfest E, Hayden M, Schultz D, Benight C (2007): False alarms and close calls: A conceptual model of warning accuracy. Weather Forecasting 22:1140-1147. doi: 10.1175/WAF1031.1

Bekryaev RV, Polyakov IV, Alexeev VA (2010) Role of polar amplification in long-term surface air temperature variations and modern Arctic warming. Journal of Climate 23:3888–3906. doi: 10.1175/2010JCLI3297.1

Boe J, Hall A, Qu X (2009) Current GCMs' Unrealistic negative feedback in the Arctic. Journal of Climate 22:4682-4695. doi: 10.1175/2009JCLI2885.1

Cavalieri D J, Parkinson CL, Gloersen P, Zwally H (1996) Sea ice concentrations from Nimbus-7 SMMR and DMSP SSM/I-SSMIS passive microwave data (updated yearly): [gsfc.nasateam.month.extent.1978-2012.n]. Boulder, Colorado USA: NASA DAAC at the National Snow and Ice Data Center

Cuffey KM, Clow GD (1997) Temperature, accumulation, and ice sheet elevation in central Greenland through the last deglacial transition. Journal of Geophysical Research 102:26383-26396.

Curry JA, Schramm JL, Ebert E (1994) Sea ice-albedo climate feedback mechanism. Journal of Climate 8:240-247.

Dakos V, Scheffer M, van Nes EH, Brovkin V, Petoukhov V, Held H (2008) Slowing down as an early warning signal for abrupt climate change. Proceedings of the National Academy of Sciences 105:14308-14312. doi/10.1073/pnas.0802430105

Ditlevsen PD, Johnsen SJ (2010) Tipping points: Early warning and wishful thinking. Geophysical Research Letters 37: L19703. doi: 10.1029.2010GL044486

Duarte CM, Lenton TM, Wadhams P, Wassmann P (2012) Abrupt climate change in the Arctic. Nature Climate Change 2:60-62.

Eisenman I, Wettlaufer JS (2009) Nonlinear threshold behavior during the loss of Arctic sea ice. Proceedings of the National Academy of Sciences 106:28-32. doi: 10.1073/pnas.0806887106

Eisenman I (2012) Factors controlling the bifurcation structure of sea ice retreat. Journal of Geophysical Research 117: D0111. doi: 10.1029/2011JD016164

Graversen RG, Wang M (2009) Polar amplification in a coupled climate model with locked albedo. Climate Dynamics 33:629-643. doi:10.1007/s00382-009-0535-6

Hall A (2003) The role of surface albedo feedback in climate. Journal of Climate 17:1550-1568.

Hartmann DL (1994) Climate sensitivity and feedback mechanisms. In: Global Physical Climatology. Academic Press, San Diego, pp 229-253.

Holland MM, Bitz CM (2003) Polar amplification of climate change in coupled models. Climate Dynamics 21:221–232. doi: 10.1007/s00382-003-0332-6

Juricke S, Goessling H, Jung T (2014) Potential sea ice predictability and the role of stochastic sea ice strength perturbations. Geophysical Research Letters 41: 8396-8403. doi: 10.1002/2014GL062081

Kattsov V, Ryabinin V, Overland J, Serreze M, Visbeck M, Walsh J, Meier W, Zhang X (2010) Arctic sea-ice change: a grand challenge of climate science. Journal of Glaciology 56(200): 1115-1121. Doi: 10.3189/002214311796406176

Knutti R, Stocker TF (2002) Limited predictability of the future thermohaline circulation close to an instability threshold. Journal of Climate 15:179-186.

Lenton TM, Held H, Kriegler E, Hall JW, Lucht W, Rahmstorf S, Schellnhuber SJ (2008) Tipping elements in the Earth's climate system. Proceedings of the National Academy of Sciences 105:1786-1793. doi: 10.1073/pnas.0705414105

Lenton TM (2012) Arctic climate tipping points. Royal Swedish Academy of Sciences 41:10-22.

Manabe S, Stouffer RJ (1980) Sensitivity of a global climate model to an increase of CO2 concentration in the atmosphere. Journal of Geophysical Research Letters 85:5529-5554

McBride J, Ebert E (2000) Verification of quantitative precipitation forecasts from operational numerical weather prediction models over Australia. Weather Forecasting 15: 103-121. doi: 10.1175/1520-0434(2000)015<0103:VOQPFF>2.0CO;2

Ogi M, Rigor IG, McPhee MG, Wallace JM (2008) Summer retreat of Arctic sea ice: role of summer winds. Journal of Geophysical Research Letters 35: L24701. doi: 10.1029/2008GL035672

Scheffer M, Bascompte J, Brock WA, Brovkin V, Carpenter SR, Dakos V, Held H, van Nes EH, Rietkerk M, Sugihara G (2009) Early-warning signals for critical transitions. Nature 461:53-59. doi: 10.1038/nature08227

Scheffer M, van Nes E, Dakos V (2015, June 1). *Early warning signals toolbox.* Retrieved from http://www.early-warning-signals.org/theory/what-is-a-critical-transition/

Stroeve et al. (2011) The Arctic's rapidly shrinking sea ice cover: a research synthesis, Climatic Change 110:1005-1027. doi: 10.1007/s10584-011-0101-1

Thompson JMT, Sieber J (2011) Predicting climate tipping as a noisy bifurcation: A review. International Journal of Bifurcation and Chaos 21: 399-423. doi: 10.1142/S0218127411028519

Timmermans ML, Proshutinsky A, Francis J, Hamilton L (2009) Taking stock of Arctic sea ice and climate. Bulletin of American Meteorological Society 90: 351–1353. http://dx.doi.org/10.1175/2009BAMS2882.1

Trenberth KE (1992) Sea ice models. In: Climate system modeling. Cambridge University Press, Cambridge, pp. 413-436.

van Nes EH, Scheffer M (2007) Slow recovery from perturbations as a generic indicator of a nearby catastrophic shift. The American Naturalist 169:738-747. doi: 10.1086/516845

van Voorn GAK (2006) *PhD mini course: introduction to bifurcation analysis,* online course materials, June 2006, Vrije University.

van Vuuren et al. (2007) Temperature increase of 21st century mitigation scenarios. Proceedings of the National Academy of Sciences 105: 15258-15262. doi: 10.1073/pnas.0711129105

Winton M (2006) Does the Arctic sea ice have a tipping point? Journal of Geophysical Research Letters 33: L23504. doi: 10.1029/2006GL028017

APPENDIX – MATLAB code for stochastic sea ice model

```
% Reference:
% Sea ice model adapted from "Nonlinear threshold behavior during the loss of Arctic
% sea ice" Eisenman and Wettlaufer, PNAS (2009)

% The MATLAB code below solves the system described by equations (2), (3) and (4)
% in the article above, using a predictor-corrector method as outlined in
% Chapter 5 of the dissertation.

% The script shown here uses the default parameters outlined in Table 1 of the
% dissertation, with the exception of the imposed surface heat flux, delta_Fo,
% which was set to 22.25 W/m^2 for the analyses discussed in the
% dissertation.

% The default configuration here runs a simulation for N=100 years at NS=100
% timesteps per year, though longer simulations were used for the early
% warning signal analysis discussed in Chapter 5 of the dissertation.
```

```
stoch=1.05;                 % level of stochastic forcing
N = 100                     % number of simulations (yr)
NS = 100;                   % number of timesteps (yr^-1)
dt = 1/NS;
t = zeros(NS*N,1);          % time (yr)
E = zeros(NS*N,1);
E(1,1) = 0;                 % Represents the energy per unit area stored in the sea ice
                            % (latent heat) when the ocean is ice-covered or in the
                            % ocean mixed layer when the ocean is ice-free (sensible
                            % heat)

t(1,1) = 0;                 % initial time

for j=1:N*NS

% Predictor
dEdt = myfunc(t(j,1),E(j,1));
E(j+1,1) = E(j,1) + dt*(dEdt + stoch*randn(1,1)/sqrt(dt));

% Corrector
dEdt = myfunc(t(j,1),E(j+1,1));
E(j+1,1) =.5*(E(j+1,1) + E(j,1) + dt*(dEdt + stoch*randn(1,1)/sqrt(dt)));
```

```
t(j+1,1) = t(j,1) + dt;

end

function dEdt=myfunc(t,E)

Li=9.5;              % latent heat of fusion of ice (W m^-3 yr)
cmlHml=6.3;          % ocean mixed layer heat capacity times depth (W m^-2 yr K^-1)
alpha_i=0.68;        % albedo for ice-covered surface
alpha_ml=0.2;        % albedo when ocean mixed layer is exposed
ki=2;                % ice thermal conductivity (W m^-1 K^-1)
Fb=2;                % heat flux into bottom of sea ie or ocean mixed layer (W m^-2)
h_alpha=0.5;         % ice thickness range; smooth transition from alpha_i to alpha_ml (m)
vo=0.1;              % dynamic transport of ice from model domain (yr^-1)
delta_Fo=22.25;      % imposed surface heat flux (W m^-2)

% Temperature-independent surface flux (W m^-2)
Fo=[110;120;120;130;94;64;61;57;54;56;64;82;110;120];

% Temperature-dependent surface flux (W m^-1 K^-1)
Ft=[3.1;3.1;3.2;3.3;2.9;2.6;2.6;2.6;2.5;2.5;2.6;2.7;3.1;3.1];

% Incident shortwave radiation flux (W m^-2)
```

```
Fs=[0;0;0;30;160;280;310;220;140;59;6.4;0;0;0];

tt = (-.5:1:12.5)/12;     %length of tt must match Fo's length

% Define ramping function R:
R=((-E)>0)*(-E);



% Define Fs, Ft, Fo:
Fsi=interp1(tt,Fs,mod(t,1));
Fti=interp1(tt,Ft,mod(t,1));
Foi=interp1(tt,Fo,mod(t,1));

% Surface temperature as described by Equation (3) for E<0
if E<0
        Targ = ( (1-alpha_i)*Fsi-Foi+delta_Fo ) / ( ki*Li/E - Fti );
        T = -(Targ>0)*Targ;
end

% Surface temperature as described by Equation (3) for E>=0
if E>=0
      T= E/cmlHml;
end
```

```
% Albedo as described by Equation (4)
alpha=0.5*(alpha_ml+alpha_i)+0.5*(alpha_ml-alpha_i)*tanh(E/(Li*h_alpha));

% Time evolution of E as described by Equation (2)
dEdt= [(1-alpha)*Fsi-Foi+delta_Fo-Fti*T+Fb+vo*R];

end
```

CURRICULUM VITAE

Dawn Kopacz

Place of birth: Port Washington, WI

Education

B.S., University of Wisconsin – Milwaukee, May 2006
Major: Atmospheric Science
Minor: Mathematics

M.S., University of Wisconsin – Milwaukee, May 2009
Major: Mathematics (Atmospheric Science concentration)

Ph.D., University of Wisconsin – Milwaukee, August 2015

Dissertation Title: Predictability of sea ice near bifurcations

Teaching and Research Experience

Graduate Teaching Assistant, UWM, 2007 – 2009, 2011 – Present

Mathematics Instructor, Alverno College, 2011 – Present

Graduate Research Assistant, UWM, 2009 – 2011

Operational Meteorologist, Innovative Weather, UWM, April 2008 – 2011

Meteorologist Intern, Innovative Weather, UWM, January - March 2008

Conference Presentations

Graduate Climate Conference, Cape Cod, MA, 2011
Topic: Long-term trends in climate models and observations

Departmental Presentations

Arctic sea ice behavior in models and observations, UWM, 2013

Honors and Awards

Graduate Teaching Assistantship, UWM, 2007– 2009, 2011– Present

Chancellor's Graduate Student Award, UWM, 2008 – Dec. 2014

Dhirendra Sikdar Scholarship, UWM, 2011 – 2012, 2008 – 2009

Mark Lawrence Teply Award, UWM, 2011

Graduate Research Assistantship, UWM, 2009 – 2011

Courses taught

Introductory Atmospheric Science (laboratory), Advanced Synoptic Meteorology (laboratory), Severe Weather (online), Quantitative Literacy, Introductory Statistics

Professional Associations

American Meteorological Society, 2009 – present

Earth Science Women's Network, 2010 – present